Title
Mechanism of Allosteric Coupling into and through the Plasma Membrane by EGFR

Journal
Cell Chemical Biology, 25(7)

ISSN
2451-9456

Authors
Sinclair, Julie KL
Walker, Allison S
Doerner, Amy E
et al.

Publication Date
2018-07-01

DOI
10.1016/j.chembiol.2018.04.005

Peer reviewed

Published in final edited form as:

Cell Chem Biol. 2018 July 19; 25(7): 857–870.e7. doi:10.1016/j.chembiol.2018.04.005.

Mechanism of allosteric coupling into and through the plasma membrane by EGFR

Julie K.L. Sinclair[†,#], **Allison S. Walker**[†,#], **Amy E. Doerner**[†], and **Alanna Schepartz**[†,§,*]

[†]Department of Chemistry, Yale University, New Haven, CT 06520-8107, USA

[§]Department of Molecular, Cellular, and Developmental Biology, Yale University, New Haven, CT 06520-8103, USA

SUMMARY

EGFR interacts through its extracellular domain (ECD) with seven different growth factors. These factors induce different structures within the cytoplasmic juxtamembrane segment (JM) of the dimeric receptor and propagate different growth factor-dependent signals to the cell interior. How this process occurs is unknown. Here we apply diverse experimental and computational tools to show that growth factor identity is encoded by the EGFR transmembrane helix (TM) into discrete helix dimer populations that differ in both cross location and cross angle. Helix dimers with smaller cross angles at multiple cross locations are decoded to induce an EGF-type coiled coil in the adjacent JM, whereas helix dimers with larger cross angles at fewer cross locations induce the TGF-α-type coiled coil. We propose an updated model for how conformational coupling across multiple EGFR domains results in growth factor-specific information transfer, and demonstrate that this model applies to both EGFR and the related receptor ErbB2.

eTOC Blurb

The mechanism by which EGFR communicates growth factor-dependent signals to the cell interior is unknown. Here we show that growth factor identity is encoded into discrete TM helix dimers. These dimers induce different coiled coil structures within the juxtamembrane region that correlate with downstream signaling.

[*]Correspondence and Lead Contact: alanna.schepartz@yale.edu.
[#]These authors contributed equally

SUPPLEMENTAL INFORMATION

Supplemental Information includes Supplemental Experimental Procedures, seven figures, and one table and can be found with this article online.

AUTHOR CONTRIBUTIONS

J.S., A.W., and A.S. designed research; J.S. and A.W. performed research; J.S., A.W., and A.S. analyzed data; J.S., A.W., A.D., and A.S. wrote the paper.

DECLARATION OF INTERESTS

The authors declare no competing interests.

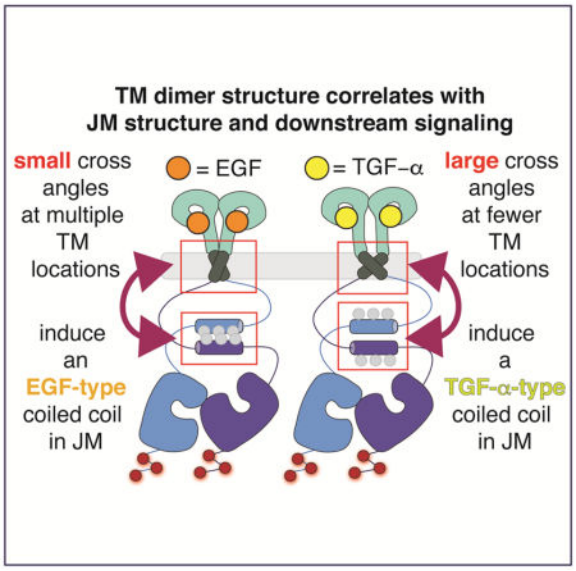

Keywords

Receptor Tyrosine Kinase (RTK); Epidermal Growth Factor Receptor (EGFR); Cancer; Transmembrane Domain; Juxtamembrane Domain; Ligand-Induced Dimerization; Signal Transduction; Allostery

INTRODUCTION

The Epidermal Growth Factor Receptor (EGFR) (Carpenter and Cohen, 1979) is a canonical receptor tyrosine kinase (RTK) with diverse roles in cell health and disease (Yarden and Sliwkowski, 2001). Like other RTKs, EGFR receives a stimulus when a growth factor binds its extracellular domain (ECD) and communicates this signal to the cell interior to initiate diverse signaling outcomes (Kovacs et al., 2015). The signal must travel faithfully over more than 200 amino acids, through a membrane-embedded transmembrane helix (TM) and the adjacent cytosolic juxtamembrane region (JM) to promote assembly of an activated, asymmetric, tyrosine kinase (TK) domain dimer (Kovacs et al., 2015; Lemmon et al., 2014). The structures of isolated ECD and TK domains (Brewer et al., 2009; Ferguson et al., 2003; Jura et al., 2009; Lu et al., 2010; Ogiso et al., 2002; Zhang et al., 2006) have been defined at high resolution, and together with computational studies (Arkhipov et al., 2013) and low-resolution EM images (Mi et al., 2011) of near full-length receptor dimers, offer preliminary clues to how individual domains cooperate and communicate as one.

Confounding the analysis of EGFR information transfer is the fact that the receptor ECD binds seven different growth factors. Different factors induce different structures locally within the isolated ECD (Arkhipov et al., 2013; Freed et al., 2017; Liu et al., 2012; Scheck et al., 2012; Wilson et al., 2009), promote different long-range structure within the cytoplasmic juxtamembrane segment (JM) (Doerner et al., 2015; Scheck et al., 2012), and propagate different growth factor-dependent signals to the cell interior (Ebner and Derynck, 1991; Roepstorff et al., 2009; Wilson et al., 2012). Growth factors EGF and HB-EGF induce

an activated EGFR whose dimeric JM coiled coil contains a Leu-rich hydrophobic interface (the 'EGF-type coiled coil), while TGF-α, AR, ER, and EPI induce a coiled coil with a polar interface (the 'TGF-α-type coiled coil) (Doerner et al., 2015) (Figure 1). JM coiled coil identity is also dictated by TK domain mutational state and pharmacologic status: the constitutively active, drug-resistant T790M/L858R EGFR dimer contains the TGF-α-type coiled coil but is transformed into the EGF-type state by class III tyrosine kinase inhibitors (Lowder et al., 2015).

It was recently proposed that biased signaling through EGFR is defined by the strength of the ligand-bound dimer, with high-affinity ligands (EGF and TGF-α) promoting strong dimers and low-affinity ligands (ER, and EPI) promoting weaker dimers (Freed et al., 2017). However, this proposal does not explain the observation that the high-affinity ligand TGF-α induces formation of the same JM coiled-coil as the low-affinity ligands ER and EPI, but not the same coiled-coil induced by high-affinity EGF (Doerner et al., 2015). Nor does it explain why cell-responses induced by TGF-α are more similar to those induced by EPI or AR than they are to those induced by EGF (Wilson et al., 2012). These inconsistencies suggest that mechanisms other than ligand-bound dimer stability and kinetics must be considered to fully understand how EGFR translates growth factor identity into cell behavior.

In this work we focus on how growth factor identity is transmitted through the EGFR TM helix to induce alternative structures within the cytoplasmic JM. Our studies begin with a chemical biology tool, bipartite tetracysteine display (Luedtke et al., 2007; Scheck and Schepartz, 2011), to confirm that EGFR activation by different growth factors leads to different structures at the inner membrane junction between the TM and JM domains. We then employed an established cysteine crosslinking assay (Lu et al., 2010) to establish the existence of two discrete TM helix populations whose identity tracks with both growth factor identity and growth factor-induced JM coiled coil structure. Guided by these results, we developed computational models of the EGFR TM-JM helix dimer that revealed a direct relationship between TM cross location and angle and the formation of alternative coiled coils within the JM. Importantly, this work identified a point mutation in the N-terminal GXXXG motif of the TM that controls JM coiled coil structure, irrespective of the identity of bound growth factor. This point mutation is found naturally within ErbB2 and accurately predicts the identity of the JM coiled coil formed within this receptor homodimer. Together, our empirical and computational results reveal how growth factor-dependent structural differences are encoded by the formation of alternative TM helix dimer populations and subsequently decoded into different JM coiled coils. These results increase our understanding of allosteric coupling within a canonical cell surface receptor.

RESULTS

Evaluating growth-factor dependent structural changes at the TM-JM junction with bipartite tetracysteine display

Our first experiments made use of bipartite tetracysteine display (Luedtke et al., 2007; Scheck and Schepartz, 2011) to test the hypothesis (Scheck et al., 2012) that growth factor-dependent structural differences within the ECD induce different TM dimer populations. This chemical biology tool makes use of the bis-arsenical dye ReAsH (Adams et al., 2002),

which becomes fluorescent only when bound to four cysteine side chains in a discrete tetracysteine motif (Walker et al., 2016). In this way, induced ReAsH fluorescence provides a readout of protein assembly and/or protein partnerships (Doerner et al., 2015; Lowder et al., 2015; Luedtke et al., 2007; Scheck et al., 2012). To apply bipartite tetracysteine display to monitor EGFR TM interactions, we made use of a previously reported EGFR variant (CC_L-1), containing Cys substitutions at two positions (648 and 649) at the TM-JM junction (Figure 1). When expressed on the cell surface, CC_L-1 binds ReAsH and fluoresces whether EGF is added to the media or not (Scheck et al., 2012). Because of the strict requirements for ReAsH fluorescence (Walker et al., 2016), this result implies that when full-length EGFR dimers are assembled on the surface of live cells, the two TM-JM junctions are proximal whether EGF is bound to the ECD or not and hence, whether the receptor exists in an active or auto-inhibited state.

In this work, we first asked whether the two EGFR TM-JM junctions would also be proximal when the ECD was bound to TGF-α in place of EGF, as these two growth factors induce the formation of different coiled coils within the JM region (Doerner et al., 2015). More broadly we wondered whether the ability of CC_L-1 to bind ReAsH and fluoresce would correlate with the induced growth factor-specific JM coiled coil structure (Doerner et al., 2015).

Growth factor-dependent changes in ECD conformation are transmitted through the membrane to the TM-JM junction and correlate with JM coiled coil structure

To evaluate whether CC_L-1 would bind ReAsH and fluoresce when activated by other growth factors, CHO-K1 cells expressing CC_L-1 or CC_H-1 (a positive control that binds ReAsH in an EGF-dependent manner (Scheck et al., 2012)) were stimulated with saturating concentrations of EGF, TGF-α, HB-EGF, BC, AR, EPI, or ER, incubated with ReAsH, washed, and immuno-stained to visualize EGFR-expressing cells. Using TIRF microscopy (TIRF-M), we quantified the level of induced ReAsH fluorescence in these cells as a function of both EGFR variant (CC_L-1 or CC_H-1) and growth factor identity (Figure 2).

As reported previously, cells expressing CC_H-1 exhibited a significant (1.5–1.7-fold) increase in ReAsH fluorescence when treated with EGF, HB-EGF, and BC, and no significant increase when treated with TGF-α, AR, ER, or EPI; cells expressing CC_L-1 exhibited a 1.4-fold increase in ReAsH fluorescence whether they were treated with EGF or not (Figure 2) (Doerner et al., 2015; Scheck et al., 2012). When cells expressing CC_L-1 were treated with TGF-α, AR, ER, or EPI, however, little or no increase in ReAsH fluorescence was observed relative to background; the only growth factor that led to a significant increase in ReAsH fluorescence was HB-EGF. Indeed, treatment of CC_L-1 with TGF-α, AR, ER, EPI, or BC led to a decrease in ReAsH fluorescence relative to untreated cells. These trends indicate that the ability of CC_L-1 to bind ReAsH and fluoresce depends on growth factor identity, and in a manner that tracks with induced JM coiled coil structure: activation by EGF and HB-EGF induces the EGF-type JM coiled coil and high levels of ReAsH fluorescence in cells expressing CC_L-1, whereas activation by TGF-α, AR, EPI, and ER induces the TGF-α-type JM coiled coil and little or no ReAsH fluorescence. The implication is that the structure of EGFR dimers at the TM-JM junction is not fixed, but rather depends

on the identity of the growth factor bound to the ECD. These observations support the hypothesis that different EGFR-activating growth factors induce different conformations in the ECD that are faithfully transmitted through the membrane, using the TM helix as a conduit (Doerner et al., 2015; Scheck et al., 2012).

Mapping growth factor-dependent changes in TM helix orientation in the membrane

In an attempt to more precisely define the growth factor-dependent changes in TM helix conformation, we made use of a previously reported (Lu et al., 2010) cysteine crosslinking assay that can detect different structures within the EGFR TM segment dimer when intact receptors are assembled on the surface of BaF3 cells. This assay employs cell lines that each stably express an EGFR variant harboring a single Cys substitution, and evaluates the extent to which each variant forms inter-chain Cys-Cys crosslinks when treated with growth factor (Figure 3A). As reported (Lu et al., 2010), when EGFR is activated by EGF, inter-chain Cys-Cys crosslinking is observed when the Cys substitution is found between residues I622 and V627, especially at A623, T624, G625 and V627 (Lu et al., 2010). If growth factor identity is communicated through the plasma membrane *via* different TM helix conformations, then the pattern of Cys crosslinking should track with growth factor identity in a manner that correlates with induced JM coiled coil structure (Doerner et al., 2015). To test this hypothesis, we evaluated the extent of inter-chain Cys-Cys crosslinking in EGFR variants harboring a single Cys substitution within the TM proper (15 variants), the ECD-TM junction (2 variants), and within the ECD at positions that are proximal in the EGF- and/or TGF-αbound dimer structure (2 variants) (Garrett et al., 2002; Ogiso et al., 2002).

The crosslinking pattern observed in the presence or absence of EGF agrees largely with previous findings (Lu et al., 2010). Without EGF treatment, little or no inter-chain Cys-Cys crosslinks were observed when the EGFR variant carried Cys at any position within the TM or the ECD (Figures 3B and S2A–B). A modest level of inter-chain Cys-Cys crosslinking was observed when the EGFR variant contained Cys substitutions within the ECD-TM junction at positions 616 and 619; these residues are predicted to be proximal in structures resulting from MD simulations of activated ECD dimers (Arkhipov et al., 2013). With EGF treatment, inter-chain Cys-Cys crosslinks were observed when the EGFR variant carried a single Cys substitution within the ECD (at positions 279 and 602), within the ECD-TM junction (at positions 616 and 619) and within the N-terminal region of the TM, with the highest crosslinks levels observed at positions 624–628. Overall, our results agree with previous crosslinking results (Lu et al., 2010), with inter-chain contacts observed in an NMR-derived structure of an EGFR TM-JM fragment in bicelles (PDB ID: 2M20; (Endres et al., 2013), and with EGFR TM interfacial distances predicted by MD simulations of the N-terminally dimerized TM domains (Arkhipov et al., 2013).

EGF and TGF-α lead to different patterns of EGFR inter-strand Cys-Cys crosslinks

Next we asked whether this crosslinking assay could detect changes in the orientation of the TM helix dimer when the EGFR ECD is bound to TGF-α in place of EGF. When cells expressing each of the EGFR single Cys variants were treated with TGF-α, inter-chain crosslinks were again observed when the EGFR variant carried Cys in the ECD, the ECD-TM junction, or in the N-terminal region of the TM, with the highest crosslinks levels

observed at positions 624–628 (Figures 3B and S3). Although the plots showing the yield of crosslinked EGFR in the presence of EGF or TGF-α are similar, clear differences are observed in the N-terminal region of the TM segment. Specifically, in the presence of TGF-α, lower levels of EGFR crosslinks are observed within the TM segment when the Cys residues are substituted at positions 626, 627, 628, and 629, and the yield of crosslinked protein was roughly constant throughout this entire region (Figures 3B and S3). Outside this one region of the TM, the levels of inter-strand crosslinks are comparable whether the cells were treated with EGF or TGF-α, suggesting that the receptor dimers themselves possess comparable overall thermodynamic stability (Freed et al., 2017).

Growth factor-dependent EGFR inter-strand Cys-Cys crosslinks patterns correlate with JM coiled coil identity

With one exception, growth factors that activate EGFR fall into two categories: EGF and HB-EGF induce formation of an activated EGFR dimer with an 'EGF-type' JM coiled coil, whereas TGF-α, AR, ER, and EPI induce an activated EGFR dimer with an alternative, 'TGF-α-type' JM coiled coil (Doerner et al., 2015) (Figure 1). If the observed differences in Cys-Cys inter-chain crosslinks within the TM identify structures that differentially transmit information through the plasma membrane, then the differences in the patterns elicited by EGF and TGF-α should be reproduced by other growth factors, and in a manner that tracks with the JM coiled coils that they each induce. To test this prediction, we performed cysteine crosslinking assays in the presence of HB-EGF and AR. We also performed experiments in which the EGFR variants were activated by BC, which induces a JM coiled coil that is an intermediate between the EGF- and TGF-αtype coiled coils (Doerner et al., 2015) (Figures 3B and S3). While concentrations of 100 nM EGF, TGF-α, HB-EGF, and BC were sufficient to activate the complete set of EGFR variants (Figure S2C), a higher concentration of 2 μM AR was required to attain comparable levels of EGFR activation (Figure S2D and E). As very high concentrations (> 4 μM) of ER or EPI were required to attain comparable levels of EGFR activation, the effect of ER and EPI were not monitored in the disulfide crosslinking assay.

As observed when cells were activated with EGF or TGF-α, the extent of Cys-Cys crosslinking at many positions–within the ECD, at the ECD-TM junction, and in the C-terminal region of the TM helix–were unaffected whether the cells were activated with EGF, TGF-α, AR, or HB-EGF (Figures 3B and S3). However, distinct differences were observed in EGFR variants containing Cys substitutions in the N-terminal region of the TM helix, especially between residues 624 and 629. In particular, the extent of Cys-Cys crosslinking in this region when cells were treated with HB-EGF and BC mirrored almost exactly the pattern observed when cells were treated with EGF, while the patterns observed when cells were treated with AR more closely resembled the pattern observed when cells were treated with TGF-α (Figures 3B and S3). The extent of Cys-Cys crosslinking was approximately equal across this region when cells were treated with TGF-α- or AR but showed a distinct preference for formation of a crosslink at positions 626–628 when cells were treated with EGF, HB-EGF, or BC. These observations suggest that activated EGFR can contain at least two different TM helix dimer populations; one population forms when the cells are treated with EGF, HB-EGF, or BC, whereas another forms when the cells are treated with TGF-α or

AR. The observed growth factor-dependent differences in Cys-Cys crosslinking within the N-terminal region of the TM support the conclusion that small but detectable (Scheck et al., 2012) growth factor-dependent changes in ECD structure propagate into structural or dynamic changes within the TM region.

It has been previously proposed that the EGFR ECD adopts growth factor-specific conformations that propagate to the TM (Freed et al., 2017; Scheck et al., 2012; Wilson et al., 2009). By overlaying structures of the dimerized human EGFR ECD in the EGF-bound (Lu et al., 2010; Ogiso et al., 2002) and TGF-α-bound (Garrett et al., 2002) states, we and others identified differences (Arkhipov et al., 2013; Liu et al., 2012; Scheck et al., 2012; Wilson et al., 2009), especially within membrane-proximal domain IV, that could propagate EGF- and TGF-α-specific conformational cues through the plasma membrane. The bipartite tetracysteine display and Cys crosslinking results reported here confirm that different ECD-bound growth factors induce different TM dimer populations. The fact the growth factor-dependent crosslink yields differ only within the TM proper, and not within the ECD or at the ECD-TM junction, implies that the effects on TM helix dimer structure and/or dynamics dominate over potential changes in overall receptor dimer stability (Freed et al., 2017). The following experiments explore how differences in the structure and/or dynamics of the TM can be decoded into different coiled coils within the JM.

Exploring whether differences in TM structure or dynamics influence JM coiled coil structure

Rosetta is an object-oriented software suite for predicting and designing protein structures, folding pathways, and protein-protein interfaces (Gray et al., 2003). The updated (Alford et al., 2015) RosettaMP framework embodies the physical and chemical properties of proteins embedded in a membrane (Alford et al., 2015; Barth et al., 2007). As our inter-chain crosslinking results imply that growth factor identity influences TM dimer structure and dynamics within the membrane, we applied RosettaMP to evaluate the breadth of dimer structures available to the TM and their influence on the assembly of the adjacent JM coiled coil. Specifically, we asked whether growth factor-dependent changes in TM structure, intimated by the previously described crosslinking data, could facilitate the formation of alternative coiled coils within the JM.

Our studies began with a high-resolution NMR structure of an EGFR TM-JM fragment (Endres et al., 2013). This structure contains the complete TM segment (residues 618 – 640) and JM region (residues 641 – 673) assembled as a dimer in bicelles (Endres et al., 2013). The structure shows the paired TM segments assembled as a parallel, α-helical dimer that crosses near the N-terminus at A629. The adjacent, paired JM region appears as an antiparallel α-helical dimer that closely resembles the NMR structure of an engineered JM peptide dimer in isolation (Jura et al., 2009) and forms on the cell surface when EGFR is activated by EGF (Scheck et al., 2012). Although other NMR-derived structures of the EGFR TM segment have since been reported (Bocharov et al., 2017; Mineev et al., 2015), the structure we used contains both the TM segment and the coiled coil-forming portion of the JM (residues R653-V665) (Endres et al., 2013).

We developed a custom workflow that employed two Rosetta scripts to model the structural relationship between the TM and the JM segments and evaluate whether growth factor-dependent differences in average TM structure could promote the formation of alternative coiled coils within the JM (Figure 4A). First, with Rosetta-MPDock (Barth et al., 2007), we generated 1,000 low energy structures for the TM helix dimer and sorted them on the basis of helix cross location and cross angle Θ. The helix cross location was defined as the TM residue with the smallest distance between paired C-α positions; this distance ranged between 3.09 Å and 47.9 Å across all 1000 structures with an average of 6.00 ± 4.29 Å (Figure S4A). The cross angle Θ was defined by drawing a vector from the C-α of each paired crossed residue to the C-α of the residue located 4 residues towards the C-terminus on the same strand and calculating the angle between the two vectors (Figure 4B).

Next, we ranked the 1000 structures obtained on the basis of the distance between paired C-α carbons at the cross location, and limited subsequent analysis to those structures whose cross location C-α to C-α distance was < 13 Å. This filter removed those structures–about 5%–whose TM segments did not appreciably interact. The remaining 950 structures were characterized by an average contact surface area of 240 ± 71 $Å^2$, a value slightly smaller than other ErbB family members, 360 ± 30 $Å^2$ (Bugge et al., 2016). Analysis of the 950 structures revealed TM helices crossed at nine locations (S621, I622, T624, G625, G628, A629, L632, V636, I640), with a significant preference for G625 (584 structures), G628 (64 structures), and A629 (169 structures) (Figure 4C). TM dimers that crossed at G625 or A629 were also characterized by the most favorable docking scores (Figure 4D). The median cross angle for structures crossed at G625 was −30.5° with a SD of 10.5° (Figure S4B), while structures crossed at G628 and A629 contained median cross angles of −42.4° ± 12.6 ° and −44.5°° ± 8.3°, respectively (Figure S4C and D). These values compare well to structurally characterized TM helix dimers, whose cross angles range between −74.3° and −10.3° for right-handed coiled coils with a median value of −25.8° (Bocharov et al., 2017; Bocharov et al., 2013; Bocharov et al., 2008a; Bocharov et al., 2010; Bragin et al., 2016; Call et al., 2010; Chen et al., 2014; Endres et al., 2013; Lau et al., 2009; MacKenzie et al., 1997; Mineev et al., 2010; Mineev et al., 2011; Mineev et al., 2014; Muhle-Goll et al., 2012; Nadezhdin et al., 2012). The lowest energy structures that crossed at positions 625, 628, and 629 were characterized by cross angles of Θ = −27.4°, −37.2° and −40.8°, respectively (Figure S4C–E). For comparison, the average cross angle observed in the NMR structure of the TM-JM dimer in bicelles (cross location A629) was −44.8° (Endres et al., 2013).

Although the preferred cross location predicted by Rosetta MPDock (G625) differed from the cross location observed by NMR of the TM-JM dimer in bicelles (A629), the two structures are extremely close: the minimum energy docked structure (crossing at G625) differed from the average NMR structure by only 3.17 Å in RMSD; this value is smaller than the RMSD among alternative experimental NMR poses, which were as large as 3.30 Å (Endres et al., 2013). Moreover, there exists a clear relationship between Rosetta energy and RMSD (Pearson's correlation coefficient $r = 0.56$ $p < 0.0001$), with 972 of the 1000 docked structures having a residual value of less than 50 Rosetta energy units in a linear regression (Figure S4E). The high correlation between the structure determined by NMR (Endres et al., 2013) and the lowest energy computational structures provides confidence that the Rosetta energy scoring function MPDock High Res 2015 (Alford et al., 2015) accurately represents

the potential energy of the EGFR TM-JM dimer system. In addition, the minimum energy docked structure we observe (which crosses at G625 with an angle of −27.4°) is virtually identical to that of a full-length EGFR structure generated by an all-atom simulation, which crosses at G625 with an angle of −31.7° (Arkhipov et al., 2013). An alternative, lower resolution modeling program TMDOCK also predicts that the TM region of EGFR can cross at G625 (Lomize and Pogozheva, 2017). More recent NMR structures of the EGFR TM also agree with these computationally modeled structures: the NMR structure of a dimeric EGFR fragment containing the TM segment and part of the JM crosses at G625 with an average cross angle of −38° or at A629 with an average cross angle of −40°(Bocharov et al., 2017). Finally, in the case of the lowest energy structures that cross at G625 or A629, we observed the expected relationship between the modeled C-α to C-α distances and experimental crosslinking yield for growth factor-treated samples (Figure 4E). The Spearman's correlation coefficient representing the relationship between the G625 C-α to C-α distance and crosslinking yield was -0.75 and −0.63 for cells treated with EGF and TGF-α, respectively; the corresponding values for structures crossed at A629 were −0.74 and −0.62. The Spearman's correlation coefficient representing the relationship between the G628 C-α to C-α distance and crosslinking yield were significantly lower, −0.34 and −0.23 for EGF and TGF-α-treated samples, respectively, suggesting that only structures that cross at G625 and A629 are biologically relevant in the context of an activated receptor. Taken together, the agreement between the RosettaMPDock models with two different NMR structures (Bocharov et al., 2017; Endres et al., 2013) and two structures generated using alternative computational approaches (Arkhipov et al., 2013), as well as with the crosslinking experiment results described herein (Figure 3), provide confidence that the Rosetta MPDock procedure accurately represents the behavior of the EGFR TM-JM region.

Monte Carlo simulations reveal effect of TM cross location and angle on JM coiled coil structure

The dihedral angles of the protein backbone remain fixed during a Rosetta-MPDock operation, and as a result the relative orientation of the TM and JM segments in a single EGFR monomer do not change. To permit the relative orientations to change, we performed 10-step Monte Carlo simulations using MPRelax (Alford et al., 2015; Barth et al., 2007; Yarov-Yarovoy et al., 2006) that allowed the JM region (residues 643 – 673) to relax while restricting the motion of the TM, and evaluated the extent to which each TM dimer orientation facilitated a transition from an EGF-type to a TGF-α-type coiled coil within the JM. To choose structures for analysis by MPRelax, we grouped the 1000 structures produced by Rosetta-MPDock on the basis of cross location and retained only those 753 structures that crossed at G625 or A629, the two favored cross locations identified by the experimental crosslinking data. We then distributed these 753 structures into √N bins on the basis of cross angle (Figure S4), where N is the number of structures that cross at that location; N = 584 for structures that cross at G625 (24 bins) and N = 169 for structures that cross at A629 (13 bins). MPRelax was then performed on the lowest energy structure in each significantly populated (>5 structures) bin. We also chose to perform MPrelax on any structures whose cross angle was greater than the median, because structures with very high cross angles have JMs that are not in contact with each other, allowing for greater conformational change in the JM during the relaxation experiment. We performed MPrelax on 30 structures in total.

Each structure was subjected to a 10-step MC simulation to generate 10,000 decoys; the decoy set was filtered with a custom script to remove structures whose JM coiled coil dimers were not antiparallel or not in contact (approximately 47%), and the remaining coiled coil dimers were categorized as EGF-type, TGF-α-like, or neither (Figures 5A and S5).

Several observations are evident upon examination of the structures that began the MC simulation crossed at G625 or A629 (Figure 5A). First, the appearance of TGF-α-type coiled coils was dependent on cross location, and were more favored when the TM helix crossed at G625 than when it crossed at A629 (Figure 5A). Second, in general, input structures with smaller cross angles at G625 (lower half) produced relaxed structures whose JM coiled coil remained in the EGF-type conformation; relaxed structures with TGF-α-type coiled coils were more prevalent among input structures with higher cross angles (Figure 5A). Although overall a relatively small number of relaxed structures containing a TGF-α-type coiled coil were observed, when the starting structure contained a TGF-α-type coiled coil and the MD simulation was repeated, 99% of the structures retained the TGF-α-type coiled coil (Figure S5C). Thus we conclude that the small number of relaxed structures containing a TGF-α-type coiled coil reflects the fact that the starting NMR structure contained an EGF-type coiled coil.

Large cross angles at G625 favor formation of a TGF-α-type coiled coil

Further examination of the relaxed structures that began the MC simulation crossed at G625 (but not A629) revealed that those structures containing a TGF-α-type coiled coil, on average, contained TM helices with larger cross angles (Figure 5B). When the final structure after MC simulation crossed at G625, the average cross angle among structures containing a TGF-α-type coiled coil was −36 ± 5 degrees; the corresponding angle among structures containing an EGF-type coiled coil was −27 ± 6 degrees. Although the distributions associated with formation of the EGF- and TGF-α-type coils overlap, the observation that larger G625 cross angles are associated with formation of a TGF-α-type coiled coil (Figure 5B) and that differences in TM helix cross location translate into differences in induced JM helix structure (Figure 5A), both support the hypothesis that TM location and cross angle contribute to JM coiled coil identity. Specifically, large cross angles at G625 promote formation of the TGF-α-type coiled coil within the JM.

Mutations in EGFR TM dimer cross locations alter JM structure and override the effect of growth factor identity

To further test the hypothesis that TM cross location and angle contribute to JM coiled coil identity, we designed EGFR variants with substitutions at positions 625, 628, and 629 within the TM (Figure 6A) and evaluated the JM coiled coil structure that formed upon growth factor activation using bipartite tetracysteine display (Figures 6B–D, S6, and S7). The first set of variants substituted G625, G628 or A629 with either a small, non-polar residue (Ala or Gly) compatible with a traditional GXXXG motif (Lemmon et al., 1994; Russ and Engelman, 2000; Senes et al., 2004) or a bulky, hydrophobic residue (Phe). The second set of variants contained two substitutions (G625I or G628V) reported to influence intracellular trafficking, an iconic differentiator of EGFR-activating growth factors on downstream biology (Heukers et al., 2013) (Figure 6A). EGFR receptors carrying G628V or G625I

substitutions exhibit dramatic or moderately reduced levels of receptor internalization, respectively, when treated with EGF (Heukers et al., 2013). In each case, the TM substitution was introduced into two validated EGFR variants, CC_H-1 and CC_H-10, that report on formation of the EGF-type and TGF-α-type JM coiled coil structures, respectively, using bipartite tetracysteine display (Doerner et al., 2015). All EGFR variants could be expressed in CHO-K1 cells, where they trafficked to the cell surface and underwent growth-factor-dependent activation as determined by the level of auto-phosphorylation on the C-terminal tail tyrosine residues and phosphorylation of Erk1/2 (Figure S6).

We first evaluated the effect of conservative substitutions at G625, G628, or A629 on coiled coil structure using bipartite tetracysteine display (Figures 6B and S7). Cells expressing variants of EGFR CC_H-1 harboring a G625A, G628A, or A629G substitution exhibited little ReAsH fluorescence in the absence of added growth factor, as expected, but showed a significant increase (1.6 to 1.7-fold) only when treated with EGF. Cells expressing variants of EGFR CC_H-10 harboring a conservative G625A, G628A, or A629G substitution also exhibited little ReAsH fluorescence in the absence of added growth factor, as expected, but showed an increase in ReAsH fluorescence (1.3 to 1.5-fold) only when treated with TGF-α. These results confirm that conservative substitutions within the TM segment, even at cross locations, have little if any effect on the transfer of information from the ECD, through the TM helix, and into the JM segment: activation of these EGFR variants with EGF led to formation of only the EGF-type JM coiled coil whereas activation with TGF-α led to formation of only the TGF-αtype JM coiled coil.

We next evaluated the effect of a non-conservative substitution of Phe at each of the three cross location residues (G625, G628, or A629). In contrast with the results obtained when these positions were substituted conservatively, EGFR variants with Phe at positions 625, 628, or 629 exhibited significant changes in preferred JM coiled coil structure. Cells expressing variants of EGFR CC_H-1 with G625F, G628F, or A629F substitutions exhibited a 1.5 to 1.8-fold increase in ReAsH fluorescence when treated with either EGF or TGF-α (Figure 6C), whereas cells expressing EGFR CC_H-10 variants with the same substitutions showed no increase in ReAsH fluorescence when treated with either EGF or TGF-α. In all three cases, substitution of a cross location residue with Phe (as in G625F, G628F, and A629F) favored EGFR dimers containing only the EGF-type JM coiled coil regardless of growth factor identity, effectively decoupling growth factor identity from JM structure. These results suggest that the EGF-type coiled coil is induced by multiple TM orientations and raise the possibility that the alternate TGF-αtype JM coiled coil is favored by a small number of highly specific TM conformations.

A hint of the TM conformation required for formation of a TGF-α-type coiled coil arose when we evaluated EGFR G625I and G628V, two EGFR variants that display aberrant receptor trafficking (Heukers et al., 2013) (Figures 6D and S7). EGFR receptors carrying the G628V mutation exhibit significantly reduced levels of receptor internalization, whereas the changes in receptors carrying the G625I mutation are smaller (Heukers et al., 2013). Consistent with these results, cells expressing EGFR CC_H-1 and CC_H-10 variants harboring the G625I substitution behave like WT EGFR: no increase in ReAsH fluorescence without added growth factor, and a significant increase (1.7-fold) upon treatment of EGFR G625I

CC_H-1 with EGF or treatment of EGFR G625I CC_H-10 with TGF-α. By contrast, cells expressing EGFR G628V versions of CC_H-1 and CC_H-10 did not behave like WT EGFR. A significant increase (1.5-fold) in ReAsH fluorescence was observed when cells expressing EGFR G628V CC_H-10 were treated with either EGF or TGF-α but not in the absence of growth factor. Cells expressing EGFR G628V CC_H-1 showed no increase in ReAsH fluorescence when treated with either EGF or TGF-α. Thus, upon activation, EGFR harboring a G628V substitution assembles into dimers containing only the polar TGF-α-type JM coiled coil, regardless of whether it is activated with EGF or TGF-α. It is remarkable that a single substitution within the TM helix–a relatively conservative substitution of Val for Gly at position 628–can alter the identity of the coiled coil formed within the adjacent JM segment, in a manner that is irrespective of growth factor identity.

Predicting the structure of the JM coiled coil within ErbB2

Over a quarter of breast cancers are characterized by ErbB2 overexpression (Hynes, 2016; Slamon et al., 1987), and ErbB2 is the only ErbB family member that does not require a growth factor to stimulate receptor homo- and hetero-dimerization and kinase activation. ErbB2 and EGFR share a high level of sequence identity within the JM segment – 68% overall and 75% within the 12-residue helix-forming JM-A region (660 to 671 in ErbB2; residues 652 to 663 in EGFR) (Figure 7A). While the two receptors share less overall sequence identity within the TM domain (20%), both contain a pair of overlapping GXXXG motifs near the N-terminus of the TM region and another near the C-terminus (Figure 7A). Moreover, the predicted structure of the ErbB2 TM homodimer–as determined by solution NMR in lipid bicelles (PDB ID: 2JWA) (Bocharov et al., 2008b) and MD simulations (Arkhipov et al., 2013)–confirm the propensity of the ErbB2 TM to form stable homodimers.

ErbB2 is also the only ErbB family member to contain a Val residue in place of Gly at position 635, corresponding to G628 in EGFR (Figure 7A) (Hynes, 2016; Slamon et al., 1987). We reasoned that if the presence of a Val at this position within the ErbB TM is necessary to specify formation of a TGF-α-type JM coiled coil within the JM (as observed with EGFR G628V), then the ErbB2 homodimer should contain a TGF-α-type JM coiled coil. To test this hypothesis, we generated variants of ErbB2 whose JM segments contained Cys substitutions at residues that corresponded to those found in EGFR CC_H-1 and CC_H-10 and used bipartite tetracysteine display to evaluate the state of the JM segment in the ErbB2 homodimers that formed. An ErbB2 variant (V635G) in which this particular Val is substituted by Gly (the residue in EGFR) was prepared as well.

The CC_H-1 and CC_H-10 versions of FLAG-tagged ErbB2 and ErbB2 V635G were expressed in transiently transfected CHO-K1 cells and showed evidence of robust auto-phosphorylation within the C-terminal tail (at Y1248, Y1221/1222, and Y877) in the absence of added growth factor that could be inhibited by Lapatinib, an ErbB2-specific tyrosine kinase inhibitor (Xia et al., 2002) (Figure S6H). Using TIRF-M, we confirmed that these cells showed evidence of ErbB2 expression on the cell surface when treated with an anti-FLAG antibody, and quantified the level of induced ReAsH fluorescence. Cells expressing ErbB2 CC_H-1 exhibited no significant increase in ReAsH fluorescence, whereas

cells expressing ErbB2 CC_H-10 exhibited a 1.8-fold increase in ReAsH fluorescence, comparable to the increase seen when EGFR CC_H-10 is treated with TGF-α(Figure 7B–C). These results confirm that the constitutively active ErbB2 homodimer contains the polar, TGF-α-type JM coiled coil and not the hydrophobic EGF-type coiled coil, as predicted.

As we observed the impact of a Val at EGFR position 628 to affect EGFR JM structure, we wondered whether the presence of Val at ErbB2 position 635 may also be sufficient in the context of ErbB2 to affect JM structure. We therefore evaluated the state of the ErbB2 JM structure in cells expressing ErbB2 CC_H-1 and CC_H-10 variants with a V635G mutation (Figure 7B and D). While cells expressing ErbB2 V635G CC_H-1 exhibited no significant increase in ReAsH fluorescence, cells expressing ErbB2 V635G CC_H-10 exhibited a 1.7-fold increase in ReAsH fluorescence, behaving just like ErbB2 CC_H-10 with a wild type TM sequence. The response of these ErbB2 variants to ReAsH indicates that Val at position 635 is sufficient in the context of EGFR to specify a TGF-αtype JM coiled coil but not within ErbB2, perhaps because of differences in the arrangement of GXXXG motifs within the EGFR and ErbB2 TM sequences. Further work will be necessary to identify which other residues in the ErbB2 TM cooperate to dictate the ErbB2 JM coiled coil preference.

DISCUSSION

Our studies define a mechanism for how growth factor specific information can be transmitted from the EGFR extracellular domain (ECD), through the membrane-embedded transmembrane segment (TM), and into the distal cytosolic juxtamembrane segment to influence diverse signaling outcomes. Our results support the theory that EGFR displays ligand functional selectivity (Wilson et al., 2009), or biased signaling, where activation by different ligands stimulate distinct receptor conformations that singularly define downstream signaling events (Kahsai et al., 2011; Liu et al., 2012). While many RTKs respond to multiple ligands and effect ligand-dependent signaling, a molecular link between the structure of the ligand-bound receptor and its distinct ligand-mediated cellular outcome has not been firmly established (Thomas et al., 2011). Here, we report direct evidence that different extracellular EGFR ligands induce distinct conformations to the intracellular transmembrane region, and that these differences translate into different JM coiled coil conformations that correlate with downstream signaling.

Our results also provide new structural details on how the EGFR TM and JM domains are conformationally coupled (Arkhipov et al., 2013; Endres et al., 2013). While it has been previously demonstrated that conformational coupling between the EGFR TM and JM domains mediates the transition between inactive and active EGFR states (Arkhipov et al., 2013; Endres et al., 2013), our work implies that specific structures adopted within the N-terminal TM homodimer allosterically dictate the conformation in the neighboring JM coiled coil complex, and in a manner that can override the identity of the growth factor bound at the ECD. Although different growth factors may induce EGFR dimers possessing different equilibrium or kinetic stability, with ER and EPI inducing EGFR dimers with low stability, and EGF and other growth factors inducing EGFR dimers with high stability (Freed et al., 2017), our experimental and computational results indicate that the TM helix conformational landscape is the primary determinant of JM coiled coil structure and hence growth factor-

dependent signaling outcome. Further, our results show how signaling output could be modulated by exogenous ligands that alter coiled coil structure, as was recently demonstrated for certain tyrosine kinase inhibitors (Lowder et al., 2015).

Our results show that growth factors fall into two main classes with respect to the population of TM dimers they induce – EGF and HB-EGF induce one family of TM structures, whereas TGF-α, AR, ER, and EPI induce another. This segregation matches how growth factors segregate with respect to induced JM structure: EGF and HB-EGF induce an EGF-type coiled coil, whereas TGF-α, AR, ER and EPI induce a TGF-α-type coiled coil (Doerner et al., 2015). This segregation also matches how growth factors segregate with respect to downstream signaling: TGF-α, AR, EPI are more likely to induce proliferation than EGF, HB-EGF, and BC (Wilson et al, 2012), and receptors bound to TGF-α, AR, EPI are recycled, while those bound to EGF, HB-EGF, and BC are degraded (Roepstorff et al, 2009). These observations of downstream signaling behavior and receptor trafficking are more consistent with growth factor classification based on TM and JM conformation than with a classification based on EGFR dimer strength (Freed et al., 2017).

How might conformational differences in the TM and/or JM regions bias signaling? First, it is possible that proteins known to bind to the JM region and induce various signaling pathways, such as calmodulin (Martin-Nieto and Villalobo, 1998), Nck adaptor protein (Hake et al., 2008), $G\alpha_S$ (Poppleton et al., 2000), PKC (Hunter et al., 1984), and $p38^{MAPK}$ (Takishima et al., 1988), are recruited preferentially by one JM conformation. Many EGFR up- and down-regulation sites are located within the JM including: a threonine phosphorylated by protein kinase C (Hunter et al., 1984; Morrison et al., 1993) and a second threonine residue phosphorylated by $p38^{MAPK}$ (Takishima et al., 1988; Winograd-Katz and Levitzki, 2006); and basolateral sorting (Guo et al., 2013) and nuclear translocation motifs (Lin et al., 2001). Different JM conformations could interact preferentially with different lipids. Lastly, alternative JM conformations could traffic differently or interact differently with the surface of the asymmetric kinase dimer to further propagate conformational changes through the kinase domains and influence differential C-terminal tail phosphorylation (Wilson et al., 2009).

Overall, our studies highlight the role of the EGFR TM domain in communicating precise activation signals through the plasma membrane by identifying subtle but distinct TM dimer populations that are directly encoded by the identity of the bound growth factor. We propose that the ability of the EGFR TM to adopt more than one N-terminal dimer conformation is the key to how EGFR translates the specific signals of multiple growth factors through the plasma membrane (Wilson et al., 2012). Conformational changes in the TM domain upon growth factor binding to the ECD have been observed in other RTKs that have multiple growth factor binding partners – for example, the binding of fibroblast growth factors FGF1 and FGF2 to the FGFR3 extracellular receptor domain promotes different distances in the C-termini of the dimerized TM domains (Sarabipour and Hristova, 2016). While our findings emphasize the significance of the TM domain for EGFR signaling, they simultaneously highlight the TM domain as a vulnerability in receptor signaling. Although oncogenic mutations in the TM domain of EGFR are underreported, pathogenic mutations located in the TM domains of other RTKs are notorious (Li and Hristova, 2006). Our approach for

using empirical and computational techniques to revise the model of EGFR TM conformational dynamics provides a generalizable strategy for expanding the structural understanding of RTK TM domains, with or without aberrant mutations.

STAR METHODS

CONTACT FOR REAGENT AND RESOURCE SHARING

Further information and requests for resources and reagents should be directed to and will be fulfilled by the Lead Contact Alanna Schepartz (Alanna.Schepartz@yale.edu).

EXPERIMENTAL MODEL AND SUBJECT DETAILS

CHO-K1 cells and BaF3 cells were transfected and cultured as indicated in method details.

METHOD DETAILS

Cell Culture—CHO-K1 cells were purchased from ATCC and maintained at 37 °C, 5% CO_2, in F12K Medium (Corning) supplemented with 10% fetal bovine serum and pen-strep (100 I.U./mL penicillin and 100 μg/mL streptomycin). Cell densities were determined with a Cellometer® Auto T4 automated counter. Transient transfection of CHO-K1 cells was performed *via* use of the TransIT-CHO Transfection Kit, according to the manufacturer's instructions (Mirus Bio LLC).

BaF3 cells were generously donated by the Springer Group (Harvard University; (Lu et al., 2010)), and maintained at 37 °C, 5% CO_2 in RPMI-1640 Medium (Invitrogen) supplemented with 10% fetal bovine serum, 10 ng/mL interleukin-3 (IL-3), and pen-strep (100 I.U./mL penicillin and 100 μg/mL streptomycin). BaF3 cells stably expressing EGFR constructs were maintained in medium that was additionally supplemented with 1 mg/mL G418. Stable transfection of BaF3 cells was performed *via* use of the Nucleofector® machine with the Amaxa® Cell Line Nucleofector® Kit V, according to the manufacturer's instructions (Lonza, Cologne, Germany). Populations of BaF3 cells stably expressing the EGFR constructs were selected/maintained by fluorescence-activated cell sorting (FACS) by immuno-staining for EGFR with an anti-EGFR antibody (AbCam product #ab231, rat monocolonal) and anti-rat AlexaFluor-647 conjugated antibody (AbCam product #ab150167, goat polyclonal) and by monitoring for GFP expression (GFP gene located in same plasmid as EGFR) (Dr. Kenneth Nelson, Yale Cell Sorting Facility).

DNA Constructs—EGFR constructs for the cysteine crosslinking and related activation assays, to be transfected into BaF3 cells, were generously donated by the Springer Group (Harvard University)(Mi et al., 2008b). Briefly, the sequences of the full-length EGFR with C-terminal protein C epitope and C-terminal hexahistidine and streptavidin binding protein affinity tags were modified into the pIRES2-GFP vector.

All other EGFR DNA constructs (for the Bipartite Tetracysteine Display and related activation assays in CHO-K1 cells) were cloned from a pcDNA3.1 plasmid, generously donated by the Kuriyan Group (University of California, Berkeley), containing the sequence of the full-length EGFR with an N-terminal FLAG tag (Scheck et al., 2012). Mutations were

introduced into the wild-type, CC_H-1, CC_H-10, or CC_L-1 EGFR sequences by use of the Quikchange Lightning site-directed mutagenesis kit (Agilent), according to the manufacturer's instructions, with the primers (purchased from Integrated DNA Technologies) listed in Table S1. DNA constructs were amplified with XL-10 Gold Ultracompetent cells (Agilent Technologies).

ErbB2 DNA constructs (for the Bipartite Tetracysteine Display and related activation assays in CHO-K1 cells) were cloned by amplifying and inserting the ErbB2 gene (from the pcDNA3.1Zeo+-Her2-YFP plasmid; (Liu et al., 2007)), generously donated by Dr. Sassa (Okinawa Institute of Science and Technology), into the pcDNA3.1 plasmid, to yield the sequence of the full-length ErbB2 with an N-terminal FLAG tag. Mutations were introduced into the wild-type ErbB2 sequences by use of Quikchange Lightning site-directed mutagenesis kit (Agilent), according to the manufacturer's instructions, with the primers (purchased from Integrated DNA Technologies) listed in Table S1. DNA constructs were amplified with XL-10 Gold Ultracompetent cells (Agilent Technologies).

Cell-Based Assays

Bipartite Tetracysteine Display Assay – i.e Surface ReAsH Labeling Studies and Total Internal Resonance Fluorescence (TIRF) Microscopy: ReAsH labeling was accomplished as described previously (Doerner et al., 2015), by treating CHO-K1 cells that were transiently transfected with EGFR or ErbB2 constructs with endocytosis inhibitors (ATP synthesis inhibition cocktail [10 mM NaN_3, 2 mM NaF, 5 mM 2-deoxy-D-glucose] or 40 μM Dynasore in F12-K media, as indicated) for 1 h at 37°C. Cells were then stimulated with/without 100 ng/mL of high-affinity growth factors (EGF (16.7 nM), TGF-α (16.7 nM), HB-EGF (10.3 nM), and BC (11.1 nM)) or 2 μg/mL of low-affinity growth factors (AR (182 nM), ER (370 nM), and EPI (333 nM)) for 30 min at 4°C, prior to labeling. Cells were then washed once with endocytosis inhibitor-containing F12K media before incubation with ReAsH labeling solution (2 μM ReAsH, 20 μM BAL in F12K media) for 60 min at 37°C. Cells were then washed and incubated with endocytosis inhibitor-containing F12K media supplemented with 100 μM BAL for 10 min at 37°C. The media was removed, and the cells were fixed using 4% paraformaldehyde for 25 min at RT. Cells were then washed with dPBS and blocked with 10% BSA in dPBS for 30 min at 37°C. Cells were then labeled with primary antibody (mouse anti-Flag, 1:1000 dilution in 10% BSA in dPBS) for 1 h at 37°C, washed three times with 10% BSA in dPBS, then incubated with secondary antibody (AlexaFlour488-conjugated goat anti-mouse, 1:2000 dilution in 10% BSA in dPBS) for 1 h at 37°C. Cells were then washed two times with 10% BSA in dPBS, washed once with dPBS, then nuclear-stained with Hoescht 33342 (1.62 μM in dPBS) for 5 min at 37°C. Cells were then washed once with dPBS and stored in dPBS at 4°C, prior to imaging.

Labeled cells were then monitored *via* TIRF microscopy, conducted on a Leica microsystems AM TIRF MC DMI6000B fitted with an EM-CCD camera (Hamamatsu) with HCX PL APO 63x/1.47 oil corrective objectives, as described previously (Doerner et al., 2015). Images were analyzed as described previously (Doerner et al., 2015; Scheck et al., 2012).

Western Blot Analysis of EGFR Autophosphorylation: Western blot analysis of EGFR autophosphorylation in transiently transfected CHO-K1 cells was accomplished as described previously (Doerner et al., 2015). CHO-K1 cells that were transiently transfected with EGFR constructs were collected (5×10^5 cells) and resuspended in 200 μL of serum free F12K media, stimulated with/without 100 ng/mL of high-affinity growth factors (EGF (16.7 nM), TGF-α (16.7 nM), HB-EGF (10.3 nM), and BC (11.1 nM)) or 2 μg/mL of low-affinity growth factors (AR (182 nM), ER (370 nM), and EPI (333 nM)) for 5 min at 37°C, pelleted, washed with serum free F12K media, pelleted, then lysed in 100 μL of lysis buffer (50 mM Tris, 150 mM NaCl, 1 mM EDTA, 1 mM NaF, 1% Triton X-100, pH 7.5, 1 x complete protease inhibitor cocktail (Roche), 1x Phos-Stop), on ice for 1 hr. Clarified cell lysates were then subjected to reducing 10% polyacrylamide SDS-PAGE electrophoresis and transferred to immuno-blot PVDF membranes. Membranes were blocked with 5% milk in TBS-T Buffer (50 mM Tris, 150 mM NaCl, 0.1% Tween, pH 7.4) for 1 hr followed by an overnight incubation at 4°C of indicated primary (rabbit or mouse) antibodies. Blots were then washed with TBS-T and incubated with either anti-rabbit or anti-mouse goat horseradish peroxidase conjugate secondary antibodies (Cell Signaling Technology) for 1 h at room temperature, then washed with TBS-T. Blots were then visualized using Clarity Western ECL reagents (BioRad), and intensities of immuno-stained bands measured with ImageJ 64 (Schneider et al., 2012).

Western blot analysis of EGFR autophosphorylation in stably transfected BaF3 cells was accomplished by collecting BaF3 cells (2×10^6 cells) and resuspending in 1 mL of serum free RPMI-1640 media for 4 h at 37°C, 5% CO_2. BaF3 cells were then treated with or without 100 nM EGF, TGF-α, HB-EGF, or BC or 2 μM AR for 5 min at 37°C, 5% CO_2 in 1 mL of serum-free RPMI-1640 media. Cells were then pelleted and washed with cold Dulbecco's PBS, twice. Cells were then then lysed with 60 μL of Lysis Buffer (25 mM HEPES, pH 7.4, 150 mM NaCl, 1% Triton X-1000, 10% glycerol, 1 mM sodium orthovanadate, 1 x complete protease inhibitor cocktail (Roche), 1x Phos-Stop), on ice for 1 hr. Clarified cell lysates were then subjected to reducing 10% polyacrylamide SDS-PAGE electrophoresis and transferred to immuno-blot PVDF membranes. Membranes were blocked with 5% milk in TBS-T Buffer (50 mM Tris, 150 mM NaCl, 0.1% Tween, pH 7.4) for 1 hr followed by an overnight incubation at 4°C of either rabbit anti-EGFR (Cell Signaling Technology, #2232) or rat anti-phospho-tyrosine (Millipore, clone 4G10) primary antibodies. Blots were then washed with TBS-T and incubated with either anti-rabbit or anti-rat goat horseradish peroxidase conjugate secondary antibodies (Cell Signaling Technology) for 1 h at room temperature, then washed with TBS-T. Blots were then visualized using Clarity Western ECL reagents (BioRad), and intensities of immuno-stained bands measured with ImageJ 64 (Schneider et al., 2012).

Western Blot Analysis of ErbB2 Autophosphorylation: Western blot analysis of ErbB2 autophosphorylation in transiently transfected CHO-K1 cells was accomplished, similarly to how EGFR autophosphorylation assays were performed (Doerner et al., 2015). CHO-K1 cells that were transiently transfected with ErbB2 constructs were collected (5×10^5 cells) and resuspended in 200 μL of serum free F12K media, then treated with/without 10 μM Lapatinib for 30 min at 37°C. Cells were then pelleted, washed with serum free F12K

media, pelleted, then lysed in 100 μL of lysis buffer (50 mM Tris, 150 mM NaCl, 1 mM EDTA, 1 mM NaF, 1% Triton X-100, pH 7.5, 1 x complete protease inhibitor cocktail (Roche), 1x Phos-Stop), on ice for 1 hr. Clarified cell lysates were then subjected to reducing 10% polyacrylamide SDS-PAGE electrophoresis and transferred to immuno-blot PVDF membranes. Membranes were blocked with 5% milk in TBS-T Buffer (50 mM Tris, 150 mM NaCl, 0.1% Tween, pH 7.4) for 1 hr followed by an overnight incubation at 4°C of indicated primary (rabbit or mouse) antibodies. Blots were then washed with TBS-T and incubated with either anti-rabbit or anti-mouse goat horseradish peroxidase conjugate secondary antibodies (Cell Signaling Technology) for 1 h at room temperature, then washed with TBS-T. Blots were then visualized using Clarity Western ECL reagents (BioRad), and intensities of immuno-stained bands measured with ImageJ 64 (Schneider et al., 2012).

Cell surface Disulfide Crosslinking Assay—BaF3 cells (2×10^6 cells) were collected and resuspended in 1 mL of serum free RPMI-1640 media for 4 h at 37°C, 5% CO_2. BaF3 cells were then treated with or without 100 nM EGF, TGF-α, HB-EGF, or BC or 2 μM AR for 5 min at 37°C, 5% CO_2 in 0.5 mL of serum-free RPMI-1640 media. Cells were then pelleted and washed with cold Dulbecco's PBS, twice. Cells were then resuspended in 45 μL of HS Buffer (25 mM HEPES, pH 7.4, 150 mM NaCl) containing 15 μg/mL of 2-bromopalmitate for 1 h at room temperature. Cells were then permeabilized by 2 cycles of freezing on dry ice for 10 min and thawing at room temperature. Permeabilized cells were treated with $CuSO_4$-o-phenanthroline (500 μM Cu(II), 2 mM 1,10- phenanthroline) at room temperature for 10 min. Cells were lysed by adding 25 μL Lysis Buffer (25 mM HEPES, pH 7.4, 150 mM NaCl, 1% Triton X-1000, 10% glycerol, 1 mM sodium orthovanadate, 1 × complete protease inhibitor cocktail with EDTA (Roche)) containing 10mM *N*-ethylmaleimide (NEM) on ice for 1 h. Clarified lysates were then subjected to non-reducing 10% polyacrylamide SDS-PAGE electrophoresis and transferred to immuno-blot PVDF membranes. Membranes were blocked with 5% milk in TBS-T Buffer (50 mM Tris, 150 mM NaCl, 0.1% Tween, pH 7.4) for 1 h, followed by an overnight incubation at 4°C of rabbit anti-EGFR (Cell Signaling Technology, #2232) primary antibody. Blots were then washed with TBS-T and incubated with anti-rabbit horseradish peroxidase conjugate secondary antibody (Cell Signaling Technology) for 1 h at room temperature, then washed with TBS-T. Blots were visualized using Clarity Western ECL reagents (BioRad), and intensities of immuno-stained bands measured with ImageJ 64 (Schneider et al., 2012). The percent of crosslinked EGFR was calculated from the equation:

$$^{\%}_{\text{X-link}} = I_{\text{X-link}}/[I_{\text{X-link}} + I_{\text{monomer}}],$$

where $I_{\text{X-link}}$ and I_{monomer} represent the intensity of the bands corresponding to the EGFR dimer (340 kD) and monomer (170 kD) molecular weights, as detected by the anti-EGFR antibody (Cell Signaling Technology, #2232).

Computational Studies

Docking of TM-JM monomers: We used the NMR structure reported by Endres et al as the starting point for our computational studies (PDBID: 2M20) on the TM-JM region of EGFR. We used the Pymol mutagenesis feature to restore the M626L mutation present in the

structure back to its native amino acid methionine. We generated the span file required for docking using the OCTOPUS server (Viklund and Elofsson, 2008) and the octopus2span script provided with Rosetta. OCTOPUS predicted that residues I622-L642 are embedded in the membrane. We then used Rosetta MPdock to generate 1,000 different docked structures of the TM-JM dimer. The following command was used to execute Rosetta MPdock:

```
mp_dock.linuxgccrelease -in:file:s PDB_FILENAME -in:file:native
<PDB_FILENAME> -in:file:fullatom -nstruct 1000 -score:weights
mpframework_docking_fa_2015.wts -mp:setup:spanfiles egfr.span -
mp:scoring:hbond -docking:partners A_B -docking:dock_pert 3 8 -
packing:pack_missing_sidechains 0
```

Where PDB_FILENAME indicates the name of the pdb file and egfr.span is the span file generated by OCTOPUS.

Choice of docked structure for relaxation simulations: The docked structures were first grouped by cross location. Because only the minimum energy structures that crossed at G625 and A629 were consistent with the observed cross-linking, we only considered structures that cross at G625 or A629 for the relaxation simulations. We then further classified structures by cross angle – structures were broken into √N groups based on their cross angle, where N is the number of structures that that cross location. Then, the lowest energy structure from each group with a cross angle greater than or equal to 27° for structures that crossed at G625 or 40.8° for structures that crossed at A629 were chos en for the starting point for a relaxation simulation. These cross angles were chosen as the smallest cross angles because they are the minimum energy cross angles for those cross positions.

Relaxation of TM-JM monomers: Structures were relaxed using the Rosetta MPrelax program. The following command was used to execute the MPrelax program:

```
rosetta_scripts.linuxgccrelease –parser:protocol SCRIPT_FILENAME –in:file:s
PDB_FILENAME –nstruct 10000 –mp:setup:spanfiles egfr.span –
mp:scoring:hbond –
relax:jump_move false –packing:pack_missing_sidechains 0 –out:pdb
```

Where SCRIPT_FILENAME is the file name of the following script, PDB_FILENAME indicates the name of the pdb file, and egfr.span is the span file generated by OCTOPUS. The script used to define the parameters of the MPrelax is:

```
<ROSETTASCRIPTS>
        <SCOREFXNS>
                <memb_hires weights= mpframework_docking_fa_2015.wts/>
        </SCOREFXNS>
        <MOVERS>
```

```
                    <AddMembraneMover name=add_memb>
                    </AddMembraneMover>
                    <MembranePositionFromTopologyMover name=init_pos>
                    </MembranePositionFromTopologyMover>
                    <FastRelax name=fast_relax scorefxn=memb_hires
repeats=10>
                              <MoveMap>
                                        <Chain number =1 chi=0 bb=0/>
                                        <Chain number =2 chi=0 bb=0/>
                                        < Jump number=1 setting=0/>
                                        <Span begin=1 end=120 chi=0 bb=0/>
                                        <Span begin=26 end=60 chi=1 bb=1/>
                                        <Span begin=86 end=120 chi=1
bb=1/>
                              </MoveMap>
                    </FastRelax>
          </MOVERS>
          <PROTOCOLS>
                    <Add mover=add_memb/>
                    <Add mover=init_pos/>
                    <Add mover=fast_relax/>
          </PROTOCOLS>
  </ROSETTASCRIPTS>
```

QUANTIFICATION AND STATISTICAL ANALYSIS

Bipartite Tetraysteine Display Assay Analysis—For bipartite tetracysteine display experiments, raw data from TIRF microscopy were analyzed using ImageJ 64 (Schneider et al., 2012). Fluorescence intensities of ReAsH and AlexaFluor 488 (EGFR levels) were quantified, and fold increase of ReAsH relative to background was normalized for EGFR expression levels. Normalized values of ReAsH fold increases were plotted with Prism version 7.0 (for Mac, GraphPad Software, La Jolla California USA, www.graphpad.com), where *n* represents number of cells quantified, and error bars represent the standard error of the mean. One-way ANOVA followed by Bonferonni multiple comparisons test was performed using GraphPad Prism version 7.0.

Cysteine Crosslinking Assay Analysis—For cysteine crosslinking experiments, raw images of the anti-EGFR stained immuno-blots were analyzed using ImageJ 64 (Schneider et al., 2012). Intensities of immuno-stained protein bands corresponding to the monomeric (170 kD) and dimeric (340 kD) EGFR molecular weights were quantified. The percent of crosslinked EGFR was then calculated from the equation: $\%_{\text{X-link}} = I_{\text{X-link}} / [I_{\text{X-link}} + I_{\text{monomer}}]$, where $I_{\text{X-link}}$ and I_{monomer} represent the intensity of the bands corresponding to the EGFR dimeric (340 kD) and monomeric (170 kD) molecular weights, as detected by the anti-EGFR antibody. Values of crosslinked EGFR were plotted with Prism version 7.0 (for Mac, GraphPad Software, La Jolla California USA, www.graphpad.com), where error bars represent the standard error of the mean of 6 independent crosslinking experiments.

Autophosphorylation Quantification Analysis—For phosphorylation experiments, raw images of the anti-EGFR- and anti-phosphotyrosine-stained immuno-blots were analyzed using ImageJ 64 (Schneider et al., 2012). Levels of autophosphorylated EGFR were calculated from the equation: pY/EGFR, where pY represents the intensity of the immuno-stained band corresponding to phosphotyrosine as detected by the anti-phosphotyrosine antibody at 170 kDa, and EGFR represents the intensity of the immuno-stained band corresponding to EGFR as detected by the anti-EGFR antibody at 170 kDa. Calculated pY/EGFR values were then normalized to the pY/EGFR value obtained from the 100 nM EGF-treated "parental" EGFR variant (C3M for the D279C/H280A, Y602C, G616C, and I619C variants; C6M for the I622C, A623C, T624C, G625C, M626C, V627C, G628C, A629C, L630C, L631C, V635C, A637C, L638C, G639C, and L642C variants). Values of pY/EGFR were plotted with Prism version 7.0 (for Mac, GraphPad Software, La Jolla California USA, www.graphpad.com), where error bars represent the standard error of the mean of 6 independent autophosphorylation experiments.

Analysis of Docking Studies—The 1,000 docked structures where then analyzed by a custom python script. The script first loads all the pdb files generated by MPdock and determines the coordinates of all C-α carbons in the pdb file. The script then calculates the distance between all matching pairs of C-α carbons from each monomer along the backbone of the TM helix (residues P620-R627). The cross location was defined as the pair of C-α carbons in the TM with the smallest distance between them. If this minimum distance was greater than 13 Å, the structure was discarded from further analysis. The cross angle was then calculated by generating one vector for each helix that started at the cross location and ended at the C-α at the i+4 position one helical turn down from the cross location. These vectors where then used to calculate the cross angle using the formula:

$$\theta = \cos^{-1} \frac{\vec{A} \cdot \vec{B}}{\|\vec{A}\| \|\vec{B}\|}$$

Where A and B are the vectors generated for each monomer. The python script used to calculate cross location and angles of the docked structures is available on request.

Analysis of Relaxation Simulations—In order to determine which of the relaxed structures formed the EGF-type- or the TGF-α-type coiled coil we wrote a script to automatically sort the structures. First the script filters out coiled coils that are not antiparallel. In order to be considered antiparallel, the distance between the C-terminal amino acid (E663) of one helix to the N-terminal amino acid of the other helix (R653) must be less than the distance between the two C-terminal amino acids of each coil. In addition the angle between vectors draw from the N- to C-terminus of each coiled coil must be greater than 90°. After filtering out coiled coils that are not antiparallel, the script classifies the remaining coiled coils based on which pair of faces of the coiled coils are closest together. The four faces of the coiled coils are defined as – face 1: L655, L659, E663; face 2: T654, L658, R662; face 3: R653, R657, E661 or R657, E661, V664; face 4: R656, Q660, L664. Classifications are based on what is known about which tetracysteine motifs bind ReAsH when EGFR is stimulated by EGF or TGF-α (Doerner et al., 2015). Coiled coils

with face 1 on the first coiled coil being closest to face 1 are defined as EGF-type. If face 3 on the first coiled coil is closest to face 3 on the second coiled then the structure is classified as TGF-α type. All other coiled coils are classified as other or ambiguous because it is not obvious which, if any CC_H motifs would be capable of binding ReAsH in these structures

DATA AND SOFTWARE AVAILABILITY

Software—PRISM 7.0 was used to process bipartite tetracysteine display assay data and make the graphs (GraphPad Software, La Jolla California USA, www.graphpad.com). The OCTOPUS server (http://octopus.cbr.su.se/) was used to predict the membrane topology of the EGFR TM-JM region. Rosetta version 2016.13 was used to perform all Rosetta simulations and all simulations were run on the Yale High Performance Computing cluster. All custom scripts were written in the Anaconda build of Python 2.7 (https://www.continuum.io/downloads) and are available at https://github.com/schepartzlab/EGFR_TM_analysis.

Data Resource—Coordinates from the NMR-derived structures of the EGFR TM-JM fragment in bicelles (PDB ID: 2M20) were utilized for computational simulations (Endres et al., 2013).

KEY RESOURCES TABLE

REAGENT or RESOURCE	SOURCE	IDENTIFIER
Antibodies		
Rabbit polyconal Anti-EGFR	Cell Signaling Technology	Cat#2232; RRID: AB_331707
Mouse monoclonal anti-Phosphotyrosine, Clone 4G10	Millipore	Cat#05-321; RRID: AB_309678
Goat polyclonal anti-Rabbit, HRP-conjugated	Cell Signaling Technology	Cat#7074; RRID: AB_2099233
Goat polyclonal anti-Mouse, HRP-conjugated	Cell Signaling Technology	Cat#7076; RRID: AB_330924
Rabbit monoclonal anti-Phospho-EGF Receptor Tyr1173 (53A5)	Cell Signaling Technology	Cat#4407; RRID: AB_331795
Rabbit polyclonal anti-Phospho-EGF Receptor Tyr1086	Cell Signaling Technology	Cat#2220; RRID: AB_823485
Rabbit polyclonal anti-Phospho-EGF Receptor Tyr 1068	Cell Signaling Technology	Cat#2234; RRID: AB_331701
Rabbit monoclonal anti-MAPK (Erk1/2) (137F5)	Cell Signaling Technology	Cat#4695; RRID: AB_390779
Rabbit polyclonal Her2/ErbB2	Cell Signaling Technology	Cat#2242; RRID: AB_331015
Rabbit polyclonal anti-Phospho-Her2/ErbB2 Tyr 1248	Cell Signaling Technology	Cat#2247; RRID: AB_331725
Rabbit monoclonal anti-Phospho-Her2/ErbB2 Tyr 1221/1222 (6B12)	Cell Signaling Technology	Cat#2243; RRID: AB_490899
Rabbit polyclonal anti-Phospho-Her2/ErbB2 Tyr 877	Cell Signaling Technology	Cat#2241; RRID: AB_2099407

REAGENT or RESOURCE	SOURCE	IDENTIFIER
Rabbit monoclonal anti-p44/42 MAPK (Erk1/2) (Thr202/Tyr204) (20G11)	Cell Signaling Technology	Cat#4376; RRID: AB_331772
Rabbit monoclonal anti-β-Actin (D6A8)	Cell Signaling Technology	Cat#8457; RRID: AB_10950489
Mouse monoclonal (M2) anti-Flag	Sigma Aldrich	Cat#F3165; RRID: AB_259529
Goat polyclonal anti-Mouse, AlexaFlour®488-conjugated	ThermoFisher Scientific	Cat#A11001; RRID: AB_2534069
Rabbit polyclonal anti-HPC4	Cell Signaling Technology	Cat#68083; AB_915040
Rat monoclonal anti-EGFR	AbCam	Cat#ab231; RRID: AB_2293306
Goat polyclonal anti-Rat, AlexaFluor®647-conjugated	AbCam	Cat#ab150167
Chemicals, Peptides, and Recombinant Proteins		
F-12K Medium	Mediatech Inc.	Cat#10-025-CV
RPMI-1640 Medium	ThermoFisher Scientific	Cat#11875-093
Fetal Bovine Serum (FBS) – Heat Inactivated	Sigma Aldrich	Cat#F4135
Penicillin/Streptomycin	ThermoFisher Scientific	Cat#15140122
Dulbecco's Phosphate Buffered Saline (dPBS)	ThermoFisher Scientific	Cat#14190
Recombinant Mouse Interleukin-3 (IL-3) carrier-free	BioLegend	Cat#575504
Non-enzymatic Cell Dissociation Solution	Sigma Aldrich	Cat#C5914
cOmplete, Mini Protease Inhibitor Tablets	Roche Applied Science	Cat#11836153001
PhosSTOP Phosphatase Inhibitor Cocktail Tablets	Roche Applied Science	Cat#04906837001
Unlabeled recombinant human Epidermal Growth Factor (EGF)	Corning	Cat#CB40052
Unlabeled recombinant human growth factors (Amphiregulin, Betacellulin, Epigen, Epiregulin, Heparin- Binding EGF)	R&D Systems, Inc.	Cat#262-AR, 261-CE, 6629-EP, 1195-EP
Unlabeled recombinant human Transforming Growth Factor-α (TGF-α)	Sigma Aldrich	Cat#T7924; CAS: 105186-99-0
CuSO4	Fisher Scientific	Cat#C493; CAS: 7758-99-8
N-ethylmaleimide	Alfa Aesar	Cat#AA40526-03; CAS: 128-53-0
1,10-phenanthroline	Acros Organics	Cat#AC157530050; CAS: 66-71-7
2-BromoPalmitic Acid	MP Biomedicals LLC	Cat#0520676601
XL-10 Gold Ultracompetent Cells	Agilent Technologies	Cat#200315
iBlot PVDF membranes	Life Technologies	Cat#IB401031

REAGENT or RESOURCE	SOURCE	IDENTIFIER
Mini-PROTEAN® TGX™ Precast Gels (10% polyacrylamide)	Bio-Rad Laboratories, Inc.	Cat#456-1036
Clarity™ Western ECL reagents	Bio-Rad Laboratories, Inc.	Cat#1705060
Glass Bottom Dishes (35 mm Dish, 14 mm Glass Diameter)	MatTek	Cat#P35G-1.5-14-C
Fibronectin	Sigma Aldrich	Cat#F1141; CAS: 86088-83-7
British Anti-Lewisite (BAL; 2,3-Dimercapto-1-propanol)	Acros Organics	Cat#AC115300250; CAS: 59-52-9
Lapatinib	Cayman Chemical Company	Cat#11493-10; CAS: 231277-92-2
Critical Commercial Assays		
Quikchange Lightning Site-Directed Mutagenesis Kit	Agilent Technologies	Cat#210519
TC-ReAsH™ II In-Cell Tetracysteine Tag Detection Kit (Red Fluorescence), for live-cell imaging	ThermoFisher Scientific	Cat#T34562
Deposited Data		
EGFR TM-JM structure in bicelles	(Endres et al., 2013)	PDB: 2M2O
Experimental Models: Cell Lines		
Hamster: CHO-K1 cells	ATCC	CRL-9618
Mouse: BaF3 cells	Laboratory of Timothy Springer; (Lu et al., 2010; Mi et al., 2008a)	N/A
Oligonucleotides		
List of mutagenesis primers used this study	This study	Table S1
Recombinant DNA		
C3M EGFR, pIERS2-GFP	Laboratory of Timothy Springer; (Lu et al., 2010; Mi et al., 2008a)	N/A
C6M EGFR, pIERS2-GFP	Laboratory of Timothy Springer; (Lu et al., 2010; Mi et al., 2008a)	N/A
Flag-tagged EGFR, pcDNA3.1	Laboratory of John Kuriyan; (Scheck et al., 2012; Zhang et al., 2006)	N/A
ErbB2-YFP, pcDNA3.1Zeo+	Laboratory of Toshihiro Sassa and Ichi Maruyama; (Liu et al., 2007)	N/A
Software and Algorithms		
Prism 7.0	GraphPad Software, La Jolla California USA	www.graphpad.com
ImageJ 64	(Schneider et al., 2012)	https://imagej.nih.gov/ij/
Rosetta version 2016.13	(Alford et al., 2015)	https://www.rosettacommons.org/
OCTOPUS membrane protein topology prediction server	(Viklund and Elofsson, 2008)	http://octopus.cbr.su.se/

REAGENT or RESOURCE	SOURCE	IDENTIFIER
Python 2.7 (Anaconda build)	Continuum Analytics, Austin, TX USA	https://www.continuum.io/downloads
Yale High Performance Computing Cluster	Yale University, CT USA	http://research.computing.yale.edu/services/high-performance-computing
Other		

Supplementary Material

Refer to Web version on PubMed Central for supplementary material.

Acknowledgments

This work was supported by the NIH (GM 83257 to A.S.). J.S. and A.W. acknowledge training support provided by the NIH (2T32GM067543) and the NSF (DGE-1122492), respectively.

References

Adams SR, Campbell RE, Gross LA, Martin BR, Walkup GK, Yao Y, Llopis J, Tsien RY. New Biarsenical Ligands and Tetracysteine Motifs for Protein Labeling in Vitro and in Vivo: Synthesis and Biological Applications. J Am Chem Soc. 2002; 124:6063–6076. [PubMed: 12022841]

Alford RF, Koehler Leman J, Weitzner BD, Duran AM, Tilley DC, Elazar A, Gray JJ. An Integrated Framework Advancing Membrane Protein Modeling and Design. PLoS Comput Biol. 2015; 11:e1004398. [PubMed: 26325167]

Arkhipov A, Shan Y, Das R, Endres Nicholas F, Eastwood Michael P, Wemmer David E, Kuriyan J, Shaw David E. Architecture and Membrane Interactions of the EGF Receptor. Cell. 2013; 152:557–569. [PubMed: 23374350]

Barth P, Schonbrun J, Baker D. Toward high-resolution prediction and design of transmembrane helical protein structures. Proc Natl Acad Sci USA. 2007; 104:15682–15687. [PubMed: 17905872]

Bocharov EV, Bragin PE, Pavlov KV, Bocharova OV, Mineev KS, Polyansky AA, Volynsky PE, Efremov RG, Arseniev AS. The Conformation of the Epidermal Growth Factor Receptor Transmembrane Domain Dimer Dynamically Adapts to the Local Membrane Environment. Biochemistry. 2017

Bocharov EV, Lesovoy DM, Goncharuk SA, Goncharuk MV, Hristova K, Arseniev AS. Structure of FGFR3 Transmembrane Domain Dimer: Implications for Signaling and Human Pathologies. Structure. 2013; 21:2087–2093. [PubMed: 24120763]

Bocharov EV, Mayzel ML, Volynsky PE, Goncharuk MV, Ermolyuk YS, Schulga AA, Artemenko EO, Efremov RG, Arseniev AS. Spatial Structure and pH-dependent Conformational Diversity of Dimeric Transmembrane Domain of the Receptor Tyrosine Kinase EphA1. J Biol Chem. 2008a; 283:29385–29395. [PubMed: 18728013]

Bocharov EV, Mayzel ML, Volynsky PE, Mineev KS, Tkach EN, Ermolyuk YS, Schulga AA, Efremov RG, Arseniev AS. Left-Handed Dimer of EphA2 Transmembrane Domain: Helix Packing Diversity among Receptor Tyrosine Kinases. Biophys J. 2010; 98:881–889. [PubMed: 20197042]

Bocharov EV, Mineev KS, Volynsky PE, Ermolyuk YS, Tkach EN, Sobol AG, Chupin VV, Kirpichnikov MP, Efremov RG, Arseniev AS. Spatial structure of the dimeric transmembrane domain of the growth factor receptor ErbB2 presumably corresponding to the receptor active state. J Biol Chem. 2008b; 283:6950–6956. [PubMed: 18178548]

Bragin PE, Mineev KS, Bocharova OV, Volynsky PE, Bocharov EV, Arseniev AS. HER2 Transmembrane Domain Dimerization Coupled with Self-Association of Membrane-Embedded Cytoplasmic Juxtamembrane Regions. J Mol Biol. 2016; 428:52–61. [PubMed: 26585403]

Brewer MR, Choi SH, Alvarado D, Moravcevic K, Pozzi A, Lemmon MA. The Juxtamembrane Region of the EGF Receptor Functions as an Activation Domain. Mol Cell. 2009; 34:641–651. [PubMed: 19560417]

Bugge K, Lindorff-Larsen K, Kragelund BB. Understanding single-pass transmembrane receptor signaling from a structural viewpoint—what are we missing? The FEBS Journal. 2016; 283:4424–4451. [PubMed: 27350538]

Call ME, Wucherpfennig KW, Chou JJ. The structural basis for intramembrane assembly of an activating immunoreceptor complex. Nat Immunol. 2010; 11:1023–U1073. [PubMed: 20890284]

Carpenter G, Cohen S. Epidermal Growth Factor. Annu Rev Biochem. 1979; 48:193–216. [PubMed: 382984]

Chen W, Gamache E, Rosenman DJ, Xie J, Lopez MM, Li YM, Wang CY. Familial Alzheimer's mutations within APPTM increase A beta 42 production by enhancing accessibility of epsilon-cleavage site. Nat Commun. 2014:5.

Doerner A, Scheck R, Schepartz A. Growth Factor Identity Is Encoded by Discrete Coiled-Coil Rotamers in the EGFR Juxtamembrane Region. Chem Biol. 2015; 22:776–784. [PubMed: 26091170]

Ebner R, Derynck R. Epidermal growth factor and transforming growth factor-a: differential intracellular routing and processing of ligand-receptor complexes. Cell Regulation. 1991; 2:599–612. [PubMed: 1777504]

Endres Nicholas F, , Das R, , Smith Adam W, , Arkhipov A, , Kovacs E, , Huang Y, , Pelton Jeffrey G, , Shan Y, , Shaw David E, , Wemmer David E. , et al. Conformational Coupling across the Plasma Membrane in Activation of the EGF Receptor. Cell. 2013; 152:543–556. [PubMed: 23374349]

Ferguson KM, Berger MB, Mendrola JM, Cho HS, Leahy DJ, Lemmon MA. EGF Activates Its Receptor by Removing Interactions that Autoinhibit Ectodomain Dimerization. Mol Cell. 2003; 11:507–517. [PubMed: 12620237]

Freed DM, Bessman NJ, Kiyatkin A, Salazar-Cavazos E, Byrne PO, Moore JO, Valley CC, Ferguson KM, Leahy DJ, Lidke DS, et al. EGFR Ligands Differentially Stabilize Receptor Dimers to Specify Signaling Kinetics. Cell. 2017; 171:1–13. [PubMed: 28938111]

Garrett TPJ, McKern NM, Lou M, Elleman TC, Adams TE, Lovrecz GO, Zhu HJ, Walker F, Frenkel MJ, Hoyne PA, et al. Crystal Structure of a Truncated Epidermal Growth Factor Receptor Extracellular Domain Bound to Transforming Growth Factor α. Cell. 2002; 110:763–773. [PubMed: 12297049]

Gray JJ, Moughon S, Wang C, Schueler-Furman O, Kuhlman B, Rohl CA, Baker D. Protein-protein docking with simultaneous optimization of rigid-body displacement and side-chain conformations. J Mol Biol. 2003; 331:281–299. [PubMed: 12875852]

Guo XL, Mattera R, Ren XF, Chen Y, Retamal C, Gonzalez A, Bonifacino JS. The Adaptor Protein-1 mu 1B Subunit Expands the Repertoire of Basolateral Sorting Signal Recognition in Epithelial Cells. Developmental Cell. 2013; 27:353–366. [PubMed: 24229647]

Hake MJ, Choowongkomon K, Kostenko O, Carlin CR, Sonnichsen FD. Specificity determinants of a novel nck interaction with the juxtamembrane domain of the epidermal growth factor receptor. Biochemistry. 2008; 47:3096–3108. [PubMed: 18269246]

Heukers R, Vermeulen JF, Fereidouni F, Bader AN, Voortman J, Roovers RC, Gerritsen HC, van Bergen en Henegouwen PMP. Endocytosis of EGFR requires its kinase activity and N-terminal transmembrane dimerization motif. J Cell Sci. 2013; 126:4900–4912. [PubMed: 23943881]

Hunter T, Ling N, Cooper JA. PROTEIN KINASE-C PHOSPHORYLATION OF THE EGF RECEPTOR AT A THREONINE RESIDUE CLOSE TO THE CYTOPLASMIC FACE OF THE PLASMA-MEMBRANE. Nature. 1984; 311:480–483. [PubMed: 6090944]

Hynes NE. ErbB2: From an EGFR Relative to a Central Target for Cancer Therapy. Cancer Research. 2016; 76:3659–3662. [PubMed: 27371737]

Kovalenko OV, Yang X, Kolesnikova TV, Hemler ME. Evidence for specific tetraspanin homodimers: inhibition of palmitoylation makes cysteine residues available for cross-linking. Biochem J. 2004; 377:407–417. [PubMed: 14556650]

Jennings BC, Nadolski MJ, Ling Y, Baker MB, Harrison ML, Deschenes RJ, Linder ME. 2-Bromopalmitate and 2-(2-hydroxy-5-nitro-benzylidene)-benzo[b]thiophen-3-one inhibit DHHC-mediated palmitoylation in vitro. J Lipid Res. 2009; 50:233–242. [PubMed: 18827284]

Jura N, Endres NF, Engel K, Deindl S, Das R, Lamers MH, Wemmer DE, Zhang X, Kuriyan J. Mechanism for Activation of the EGF Receptor Catalytic Domain by the Juxtamembrane Segment. Cell. 2009; 137:1293–1307. [PubMed: 19563760]

Kahsai AW, Xiao KH, Rajagopal S, Ahn S, Shukla AK, Sun JP, Oas TG, Lefkowitz RJ. Multiple ligand-specific conformations of the beta(2)-adrenergic receptor. Nature Chemical Biology. 2011; 7:692–700. [PubMed: 21857662]

Kovacs E, Zorn JA, Huang Y, Barros T, Kuriyan J. A Structural Perspective on the Regulation of the Epidermal Growth Factor Receptor. Annu Rev Biochem. 2015; 84:739–764. [PubMed: 25621509]

Lau TL, Kim C, Ginsberg MH, Ulmer TS. The structure of the integrin alpha IIb beta 3 transmembrane complex explains integrin transmembrane signalling. Embo J. 2009; 28:1351–1361. [PubMed: 19279667]

Lemmon MA, Schlessinger J, Ferguson KM. The EGFR Family: Not So Prototypical Receptor Tyrosine Kinases. Cold Spring Harb Perspect Biol. 2014; 6:1–18.

Lemmon MA, Treutlein HR, Adams PD, Brunger AT, Engelman DM. A dimerization motif for transmembrane [alpha]-helices. Nat Struct Mol Biol. 1994; 1:157–163.

Li E, Hristova K. Role of Receptor Tyrosine Kinase Transmembrane Domains in Cell Signaling and Human Pathologies†. Biochemistry. 2006; 45:6241–6251. [PubMed: 16700535]

Lin SY, Makino K, Xia WY, Matin A, Wen Y, Kwong KY, Bourguignon L, Hung MC. Nuclear localization of EGF receptor and its potential new role as a transcription factor. Nature Cell Biology. 2001; 3:802–808. [PubMed: 11533659]

Liu P, Cleveland TE, Bouyain S, Byrne PO, Longo PA, Leahy DJ. A single ligand is sufficient to activate EGFR dimers. Proc Natl Acad Sci USA. 2012

Liu P, Sudhaharan T, Koh RML, Hwang LC, Ahmed S, Maruyama IN, Wohland T. Investigation of the Dimerization of Proteins from the Epidermal Growth Factor Receptor Family by Single Wavelength Fluorescence Cross-Correlation Spectroscopy. Biophys J. 2007; 93:684–698. [PubMed: 17468161]

Lomize AL, Pogozheva ID. Proteome-Wide Modeling of Transmembrane Alpha-Helical Homodimers by TMDOCK. Biophys J. 2017; 112:358a.

Lowder MA, Doerner AE, Schepartz A. Structural Differences between Wild-Type and Double Mutant EGFR Modulated by Third-Generation Kinase Inhibitors. J Am Chem Soc. 2015; 137:6456–6459. [PubMed: 25973741]

Lu C, Mi LZ, Grey MJ, Zhu J, Graef E, Yokoyama S, Springer TA. Structural Evidence for Loose Linkage between Ligand Binding and Kinase Activation in Epidermal Growth Factor Receptor. Mol Cell Biol. 2010; 30:5432–5443. [PubMed: 20837704]

Luedtke NW, Dexter RJ, Fried DB, Schepartz A. Surveying polypeptide and protein domain conformation and association with FlAsH and ReAsH. Nat Chem Biol. 2007; 3:779–784. [PubMed: 17982447]

MacKenzie KR, Prestegard JH, Engelman DM. A transmembrane helix dimer: Structure and implications. Science. 1997; 276:131–133. [PubMed: 9082985]

Martin-Nieto J, Villalobo A. The human epidermal growth factor receptor contains a juxtamembrane calmodulin-binding site. Biochemistry. 1998; 37:227–236. [PubMed: 9425043]

Mi LZ, Grey MJ, Nishida N, Walz T, Lu C, Springer TA. Functional and Structural Stability of the Epidermal Growth Factor Receptor in Detergent Micelles and Phospholipid Nanodiscs. Biochemistry. 2008a; 47:10314–10323. [PubMed: 18771282]

Mi LZ, Grey MJ, Nishida N, Walz T, Lu C, Springer TA. Functional and Structural Stability of the Epidermal Growth Factor Receptor in Detergent Micelles and Phospholipid Nanodiscs†. Biochemistry. 2008b; 47:10314–10323. [PubMed: 18771282]

Mi LZ, Lu C, Li Z, Nishida N, Walz T, Springer TA. Simultaneous visualization of the extracellular and cytoplasmic domains of the epidermal growth factor receptor. Nat Struct Mol Biol. 2011; 18:984–989. [PubMed: 21822280]

Mineev KS, Bocharov EV, Pustovalova YE, Bocharova OV, Chupin VV, Arseniev AS. Spatial Structure of the Transmembrane Domain Heterodimer of ErbB1 and ErbB2 Receptor Tyrosine Kinases. J Mol Biol. 2010; 400:231–243. [PubMed: 20471394]

Mineev KS, Bocharov EV, Volynsky PE, Goncharuk MV, Tkach EN, Ermolyuk YS, Schulga AA, Chupin VV, Maslennikov IV, Efremov RG, et al. Dimeric Structure of the Transmembrane Domain of Glycophorin A in Lipidic and Detergent Environments. Acta Naturae. 2011; 3:90–98. [PubMed: 22649687]

Mineev KS, Goncharuk SA, Arseniev AS. Toll-like receptor 3 transmembrane domain is able to perform various homotypic interactions: An NMR structural study. Febs Lett. 2014; 588:3802–3807. [PubMed: 25217833]

Mineev KS, Panova SV, Bocharova OV, Bocharov EV, Arseniev AS. The Membrane Mimetic Affects the Spatial Structure and Mobility of EGFR Transmembrane and Juxtamembrane Domains. Biochemistry. 2015; 54:6295–6298. [PubMed: 26440883]

Morrison P, Takishima K, Rosner MR. ROLE OF THREONINE RESIDUES IN REGULATION OF THE EPIDERMAL GROWTH-FACTOR RECEPTOR BY PROTEIN-KINASE-C AND MITOGEN-ACTIVATED PROTEIN-KINASE. J Biol Chem. 1993; 268:15536–15543. [PubMed: 8393447]

Muhle-Goll C, Hoffmann S, Afonin S, Grage SL, Polyansky AA, Windisch D, Zeitler M, Burck J, Ulrich AS. Hydrophobic Matching Controls the Tilt and Stability of the Dimeric Platelet-derived Growth Factor Receptor (PDGFR) beta Transmembrane Segment. J Biol Chem. 2012; 287:26178–26186. [PubMed: 22619173]

Nadezhdin KD, Bocharova OV, Bocharov EV, Arseniev AS. Dimeric structure of transmembrane domain of amyloid precursor protein in micellar environment. Febs Lett. 2012; 586:1687–1692. [PubMed: 22584060]

Ogiso H, Ishitani R, Nureki O, Fukai S, Yamanaka M, Kim JH, Saito K, Sakamoto A, Inoue M, Shirouzu M, et al. Crystal Structure of the Complex of Human Epidermal Growth Factor and Receptor Extracellular Domains. Cell. 2002; 110:775–787. [PubMed: 12297050]

Poppleton HM, Sun H, Mullenix JB, Wiepz GJ, Bertics PJ, Patel TB. The juxtamembrane region of the epidermal growth factor receptor is required for phosphorylation of G alpha(s). Archives of Biochemistry and Biophysics. 2000; 383:309–317. [PubMed: 11185568]

Roepstorff K, Grandal MV, Henriksen L, Knudsen SLJ, Lerdrup M, Grøvdal L, Willumsen BM, van Deurs B. Differential Effects of EGFR Ligands on Endocytic Sorting of the Receptor. Traffic. 2009; 10:1115–1127. [PubMed: 19531065]

Russ WP, Engelman DM. The GxxxG motif: A framework for transmembrane helix-helix association. J Mol Biol. 2000; 296:911–919. [PubMed: 10677291]

Sarabipour S, Hristova K. Mechanism of FGF receptor dimerization and activation. Nat Commun. 2016; 7:10262. [PubMed: 26725515]

Scheck RA, Lowder MA, Appelbaum JS, Schepartz A. Bipartite Tetracysteine Display Reveals Allosteric Control of Ligand-Specific EGFR Activation. ACS Chem Biol. 2012; 7:1367–1376. [PubMed: 22667988]

Scheck RA, Schepartz A. Surveying Protein Structure and Function Using Bis-Arsenical Small Molecules. Acc Chem Res. 2011; 44:654–665. [PubMed: 21766813]

Schneider CA, Rasband WS, Eliceiri KW. NIH Image to ImageJ: 25 years of image analysis. Nat Methods. 2012; 9:671–675. [PubMed: 22930834]

Senes A, Engel DE, DeGrado WF. Folding of helical membrane proteins: the role of polar, GxxxG-like and proline motifs. Curr Opin Struct Biol. 2004; 14:465–479. [PubMed: 15313242]

Slamon DJ, Clark GM, Wong SG, Levin WJ, Ullrich A, McGuire WL. Human breast cancer: correlation of relapse and survival with amplification of the HER-2/neu oncogene. Science. 1987:235.

Takishima K, Friedman B, Fujiki H, Rosner MR. THAPSIGARGIN, A NOVEL PROMOTER, PHOSPHORYLATES THE EPIDERMAL GROWTH-FACTOR RECEPTOR AT THREONINE-669. Biochemical and Biophysical Research Communications. 1988; 157:740–746. [PubMed: 3202876]

Thomas C, Moraga I, Levin D, Krutzik PO, Podoplelova Y, Trejo A, Lee C, Yarden G, Vleck SE, Glenn JS, et al. Structural Linkage between Ligand Discrimination and Receptor Activation by Type I Interferons. Cell. 2011; 146:621–632. [PubMed: 21854986]

Viklund H, Elofsson A. OCTOPUS: improving topology prediction by two-track ANN-based preference scores and an extended topological grammar. Bioinformatics. 2008; 24:1662–1668. [PubMed: 18474507]

Walker AS, Rablen PR, Schepartz A. Rotamer-Restricted Fluorogenicity of the Bis-Arsenical ReAsH. J Am Chem Soc. 2016; 138:7143–7150. [PubMed: 27163487]

Webb Y, Hermida-Matsumoto L, Resh MD. Inhibition of Protein Palmitoylation, Raft Localization, and T Cell Signaling by 2-Bromopalmitate and Polyunsaturated Fatty Acids. J Biol Chem. 2000; 275:261–270. [PubMed: 10617614]

Wilson KJ, Gilmore JL, Foley J, Lemmon MA, Riese DJI. Functional selectivity of EGF family peptide growth factors: Implications for cancer. Pharmacol Ther. 2009; 122:1–8. [PubMed: 19135477]

Wilson KJ, Mill C, Lambert S, Buchman J, Wilson TR, Hernandez-Gordillo V, Gallo RM, Ades LMC, Settleman J, Riese DJ. EGFR ligands exhibit functional differences in models of paracrine and autocrine signaling. Growth Factors. 2012; 30:107–116. [PubMed: 22260327]

Winograd-Katz SE, Levitzki A. Cisplatin induces PKB/Akt activation and p38(MAPK) phosphorylation of the EGF receptor. Oncogene. 2006; 25:7381–7390. [PubMed: 16785992]

Xia W, Mullin RJ, Keith BR, Liu LH, Ma H, Rusnak DW, Owens G, Alligood KJ, Spector NL. Anti-tumor activity of GW572016: a dual tyrosine kinase inhibitor blocks EGF activation of EGFR/erbB2 and downstream Erk1/2 and AKT pathways. Oncogene. 2002; 21:6255–6263. [PubMed: 12214266]

Yarden Y, Sliwkowski MX. Untangling The ErbB Signalling Network. Nat Rev Mol Cell Biol. 2001; 2:127–137. [PubMed: 11252954]

Yarov-Yarovoy V, Schonbrun J, Baker D. Multipass membrane protein structure prediction using Rosetta. Proteins. 2006; 62:1010–1025. [PubMed: 16372357]

Zhang X, Gureasko J, Shen K, Cole PA, Kuriyan J. An Allosteric Mechanism for Activation of the Kinase Domain of Epidermal Growth Factor Receptor. Cell. 2006; 125:1137–1149. [PubMed: 16777603]

Significance

The Epidermal Growth Factor Receptor (EGFR) is critical to the biology of many common epithelial cancers, and since its discovery has served as a model for understanding how information is transmitted through the plasma membrane to affect diverse signaling outcomes. EGFR interacts through its extracellular domain (ECD) with seven different growth factors. These factors induce different structures within the cytoplasmic juxtamembrane segment (JM) of the dimeric receptor and propagate different growth factor-dependent signals to the cell interior. How this process occurs is unknown. Here we apply diverse experimental and computational tools to show that the identity of the growth factor bound to the EGFR ECD is encoded by the EGFR transmembrane helix (TM) into discrete helix dimer populations that differ in both cross location and cross angle. Helix dimers with smaller cross angles at multiple cross locations are decoded to induce one coiled coil in the adjacent JM, whereas helix dimers with larger cross angles at fewer cross locations induce an alternative coiled coil. Our results reveal a direct correlation between TM helix population, downstream signaling, and JM coiled coil conformation, and allow us to accurately predict the JM coiled coil structure in the related ErbB2 homodimer. We propose an updated model for how conformational coupling across multiple EGFR domains results in growth factor-specific information transfer, and demonstrate that this model applies to both EGFR and the related receptor ErbB2. The empirical and computational approach used to revise the model of EGFR TM conformational dynamics represents a generalizable strategy for expanding the structural and energetic understanding of RTK TM domains, with or without aberrant mutations, that could inform the design of selective inhibitors.

Highlights

- Different activating growth factors induce different TM dimer structures in EGFR.
- Growth factor-dependent TM dimers differ in both cross location and angle.
- TM dimer structure correlates with JM structure and downstream signaling.
- Conformational coupling across EGFR domains communicates growth factor identity.

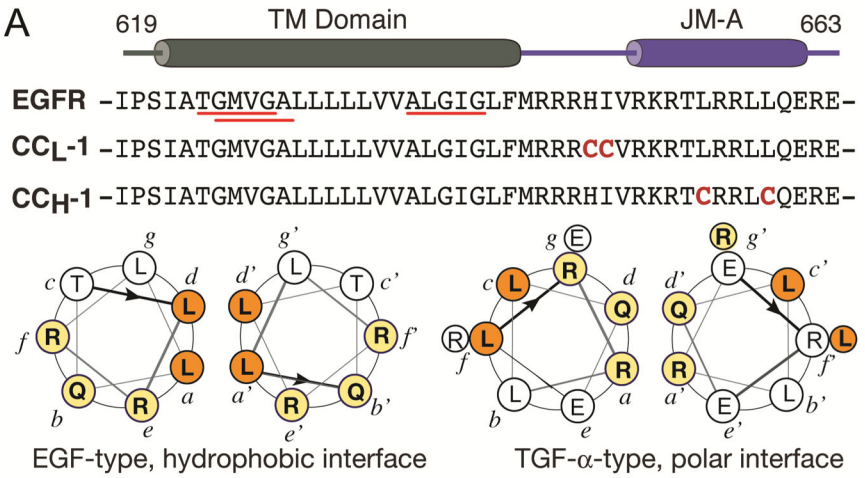

Figure 1. Monitoring growth factor-dependent assembly at the TM-JM junction using bipartite tetracysteine display

Sequence of the transmembrane (TM) and juxtamembrane (JM) regions of WT EGFR alongside those of EGFR CC_H-1 and CC_L-1. GXXXG motifs are identified by orange lines. The helical wheel diagrams show axial views of inter-helix packing in EGF-type and TGF-α-type coiled coils.

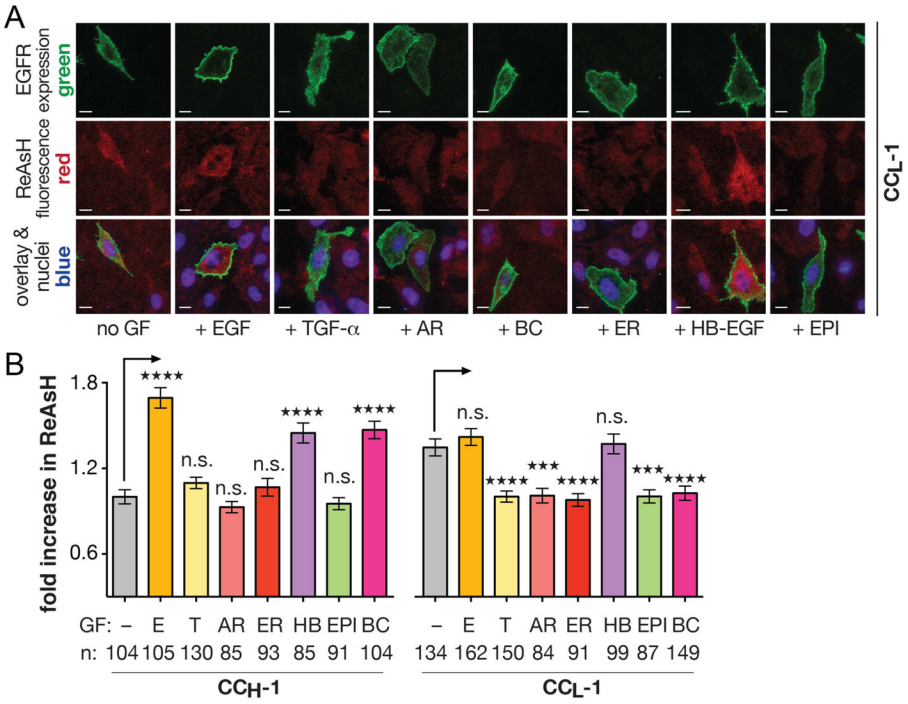

Figure 2. EGFR TM-JM junction structure is growth factor-dependent

(A) Representative TIRF-M images of cells illustrating ReAsH labeling (red fluorescence) and FLAG-tagged CC_L-1 EGFR expression (green fluorescence) in the absence or presence of EGF, TGF-α, BC, HB-EGF (100 ng/mL) or AR, ER, or EPI (2 μg/mL). Scale bars represent 10 μm. (B) Quantification of TIRF-M results, from "n" cells, as a fold increase in expression-corrected ReAsH fluorescence over background. Error bars represent SEM. ***p<0.001 and ****p<0.0001 from one-way ANOVA with Bonferroni post-analysis accounting for multiple comparisons. For detection of growth factor-stimulated phosphorylation of EGFR (CC_L-1 and CC_H-1) and Erk, see Figure S1.

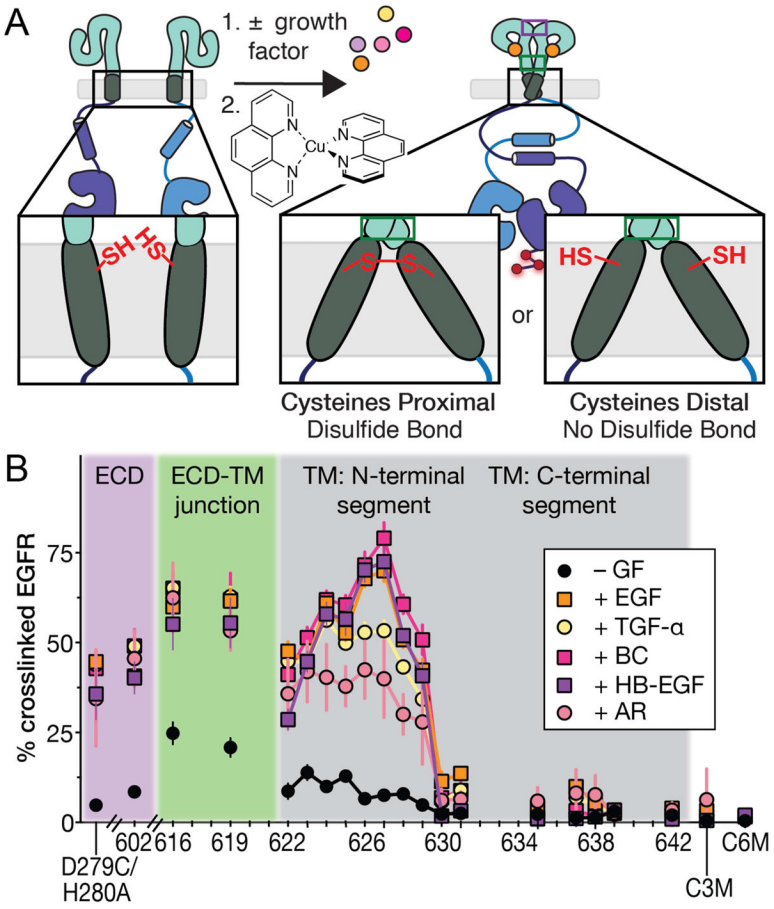

Figure 3. EGFR TM dimer structure is growth factor-dependent

(A) Experimental scheme. EGFR variants containing a single Cys within the ECD or TM are treated with growth factor and Cu(II)-1,10-phenanthroline. Cys residues proximal in a growth factor-induced TM dimer form disulfide bonds whereas distal residues do not. (B) Plot illustrating the % crosslinked EGFR observed in cells expressing each Cys variant. Values shown represent the average of six biological replicates; the error bar represents SEM. The observed crosslinking pattern was unaffected by antibody identity (anti-EGFR *vs.* anti-HPC4) (Figure S2B). See also Figures S2 and S3.

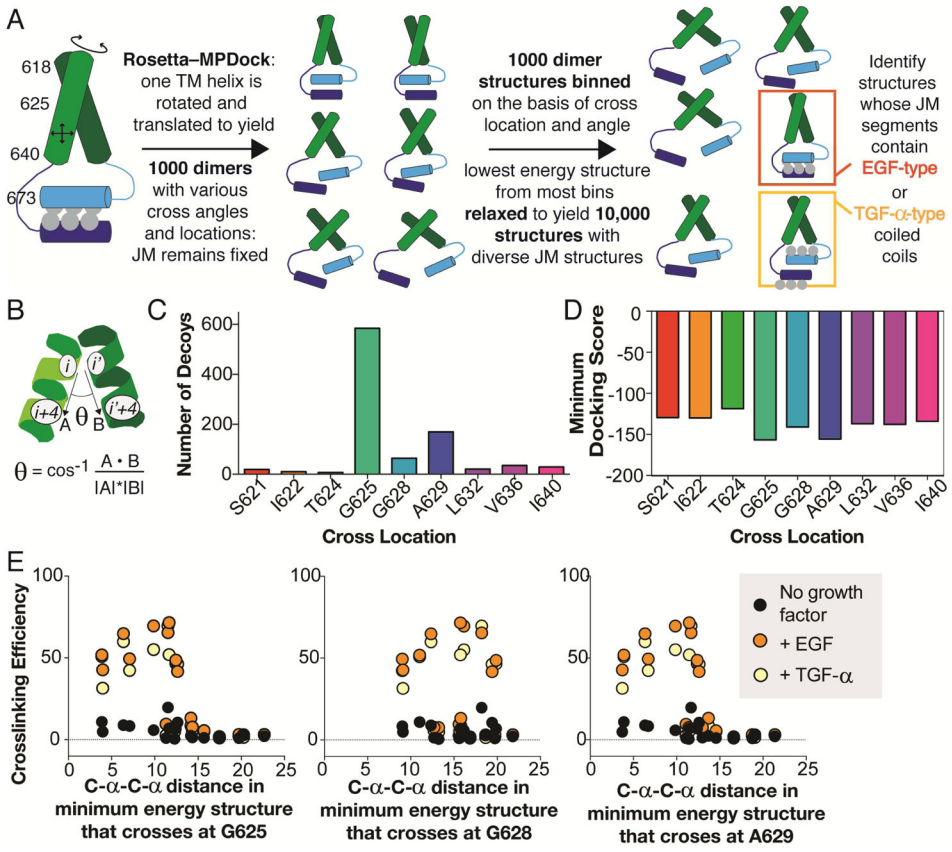

Figure 4. Computational modeling of the EGFR TM

(A) Rosetta MPdock and MPrelax were used to model the EGFR TM-JM conformational landscape. (B) Cross angles were calculated from vectors draw from the cross position (i) to the residue one turn down the helix (i+4). (C) Distribution of cross locations predicted by Rosetta MPdock. (D) Minimum docking score of the lowest energy structure crossed at each location shown. (E) Correlation between the observed experimental crosslinking efficiency at each TM position (Figure 3B) and the C-α-C-α distance in the minimum energy structure that crosses at G625, G628, or A629. See also Figure S4.

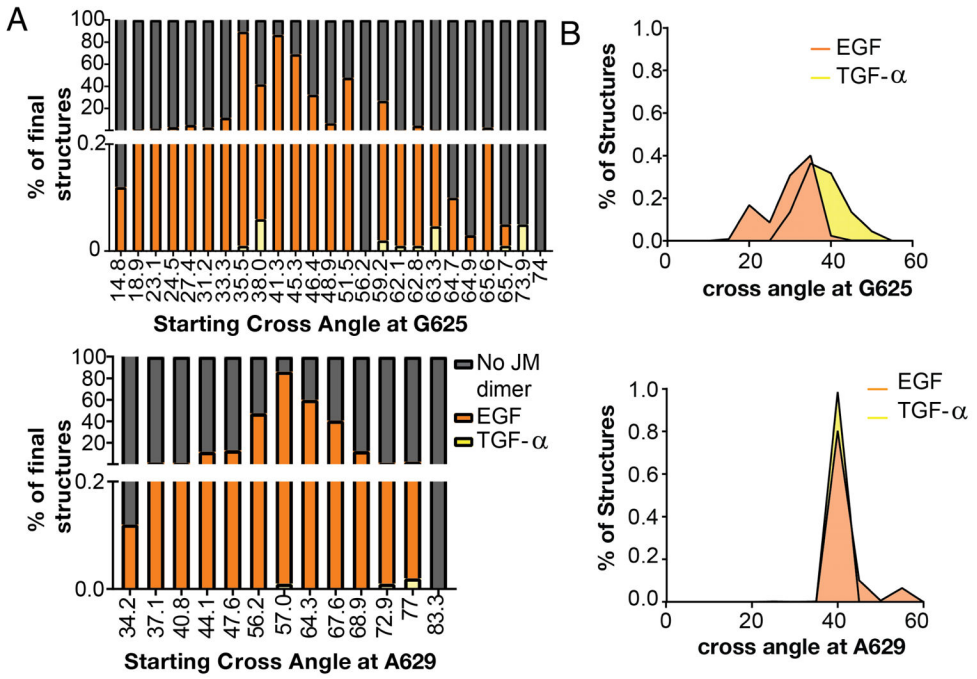

Figure 5. Relaxation of docked structures

(A) Plots illustrating how the magnitude of the cross angle at G625 and A629 prior to relaxation influences JM coiled coil identity after relaxation is complete. (B) Plots illustrating the distribution of cross angle magnitudes at G625 and A629 in output structures containing EGF- or TGF-α-type coiled coils. See also Figure S5.

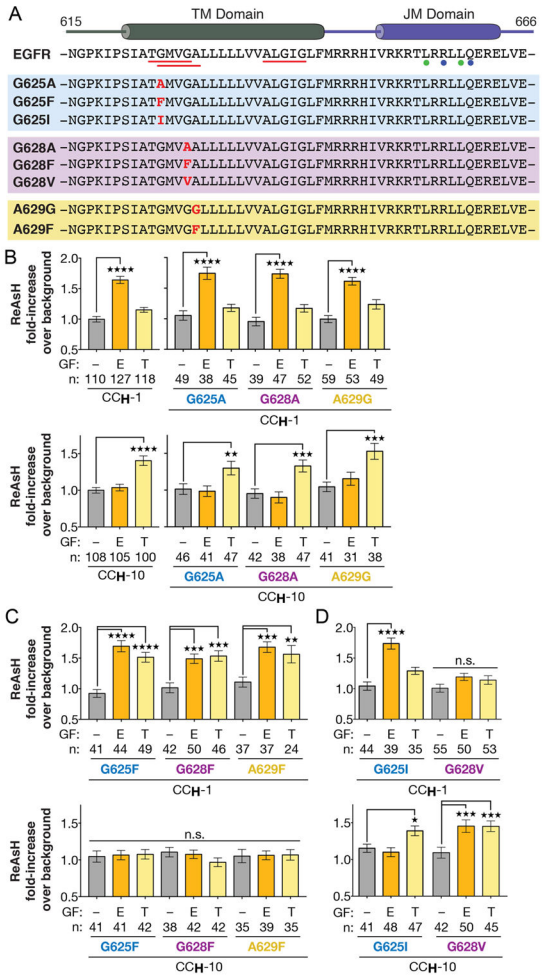

Figure 6. Point mutations within the TM can influence JM coiled coil structure

(A) Sequences of the TM and JM regions of WT and variants with point mutations within the TM. GXXXG motifs are noted with orange lines. JM residues substituted with Cys in CC_H-1 or CC_H-10 EGFR are indicated with green (L655 and L659) or blue dots (R656 and Q660), respectively. (B–D) Quantification of TIRF-M results, from "n" cells, as a fold increase in expression-corrected ReAsH fluorescence over background of CHO-K1 cells expressing CC_H-1 or CC_H-10 EGFR, when treated with/without EGF or TGF-α (100 ng/mL). Error bars represent SEM. *p<0.1, **p< 0.01, ***p<0.001 and ****p<0.0001 from one-way ANOVA with Bonferroni post-analysis accounting for multiple comparisons. See also Figures S6 and S7; and Table S1.

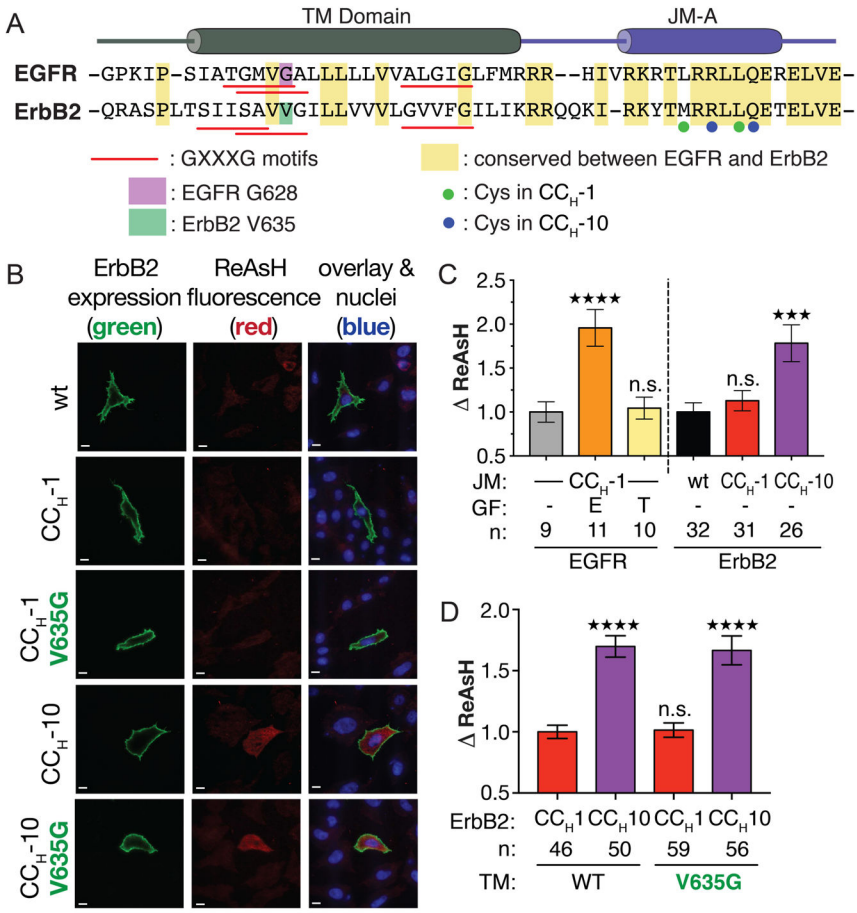

Figure 7. The ErbB2 homodimer contains only a TGF-α-type coiled coil within the JM

(A) Sequences of the TM and JM regions of WT EGFR and ErbB2. GXXXG motifs are noted with orange lines. Conserved residues are highlighted in yellow. JM residues substituted with Cys in CC_H-1 or CC_H-10 ErbB2 are indicated with green (M663 and L667) or blue dots (R665 and Q668), respectively. (B) Representative TIRF-M images of CHO-K1 cells expressing FLAG-tagged WT or V635G CC_H-1 and CC_H-10 ErbB2 after ReAsH treatment. Scale bars represent 10 μm. (C and D) Quantification of TIRF-M results, from "n" number of cells, as a fold increase in expression-corrected ReAsH fluorescence over background of CHO-K1 cells expressing WT, CC_H-1, or CC_H-10 ErbB2 (with/without a V635G mutation in the TM domain). Error bars represent SEM. ***p<0.001 and ****p<0.0001 from one-way ANOVA with Bonferroni post-analysis accounting for multiple comparisons. See also Figure S6 and Table S1.